JCTC Journal of Chemical Theory and Computation

Article

pubs.acs.org/JCTC

Computational Prediction of Structures and Optical Excitations for Nanoscale Ultrasmall ZnS and CdSe Clusters

Kiet A. Nguyen,*[,†,‡] Ruth Pachter,*[,†] and Paul N. Day[†,§]

[†]Air Force Research Laboratory, Wright-Patterson Air Force Base, Ohio 45433, United States

[‡]UES, Inc., Dayton, Ohio 45432, United States

[§]General Dynamics Information Technology, Inc., Dayton, Ohio 45431, United States

Supporting Information

ABSTRACT: Small semiconductor nanoclusters are important for understanding the initial formation and growth of quantum dots and also for application, for example in the tunability provided by size. However, electronic structures and effects of capping ligands have not been systematically characterized. Thus, ground and excited state calculations using coupled-cluster methods were carried out to provide benchmarks for evaluating the applicability of density functional theory (DFT) and time-dependent DFT (TDDFT) with different functionals for the ground and excited states, respectively. Our computed data suggests that the popular B3LYP functional does not deliver optimal results for the ground and excited state. While the PBE0 functional was found to provide a good description for both the ground and excited states for small bare $(ZnS)_n$ and bare and ligated $(CdSe)_n$ clusters, the results for the hydrated $(ZnS)_n$ clusters were found to deteriorate significantly. However, the errors appear to decrease with increasing cluster size. Excitation energies obtained with the long-range hybrid CAM-B3LYP and CA-B3LYP were found to provide more consistent results for both anhydrous and hydrated $(ZnS)_n$ clusters. However, their performance in spectral predictions for larger clusters requires further study. Using PBE0, electronic structures of the ground and excited states for $(ZnS)_n$ and $(CdSe)_n$ up to $n = 37$ using DFT and TDDFT, respectively, were re-examined. With the exception of the cage−core $(ZnS)_{13}$, $(CdSe)_{13}$, and $(CdSe)_{14}$, small $(ZnS)_n$ and $(CdSe)_n$ are predicted to be spheroids and tubular structures (6, 8−12, 15−19) with squares and hexagons, similar to the structures of carbon single-wall nanotubes. Wurtzite ($n = 23$−27, 36, 37) and cage−core ($n = 29$−35) structures are energetically more favorable for larger clusters. We find that water and amines increase the intensities and blue shift the excitations of bare clusters. One photon absorption spectra predicted by TDDFT with the PCM solvation model for $(CdSe\text{-methylamine})_{13}$ and the larger ligated $(CdSe)_{33}$ are consistent with the experimental spectra.

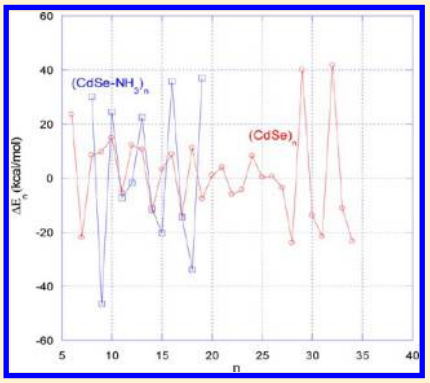

1. INTRODUCTION

Colloidal semiconductor quantum dots (QDs) have drawn much attention for application due to their size and composition-dependent properties.[1−5] For example, compared to nonlinear absorbing materials based on organic chromophores, semiconductor quantum dots have a large two-photon absorption cross-section and better photostability.[6,7] Interestingly, the desired tunability in excitation could be enabled by ultrasmall quantum dots, or so-called semiconductor nanoclusters (SNCs). However, although focusing SNC sizes with various ligands has been a topic of growing interest,[8−12] including in aqueous solution,[13−16] as reviewed,[17] available experimental spectra for small clusters is scarce. It has been postulated by Evans et al.[18] that there are two driving forces for growth of II−VI QDs, namely the step-growth mechanism and a living chain-addition-like polymerization, which results in a larger range of sizes with better monodispersity. This can be achieved by an excess of anionic ligand, which causes cluster dissolution at the appropriate temperature, and subsequent reaction with clusters in solution to produce larger QDs with time.[18] On the other hand, the step-growth-type mechanism in the absence of excess ligand is responsible for quantized growth. Thermodynamically stable SNCs observed in synthesis of colloidal QDs can be considered as building blocks for assemblies, e.g. the lamellar assembly of so-called quantum belts.[12]

At the same time, theoretical investigation of SNC morphology, effects of passivation by various ligands, and calculation of optical excitation in some cases was undertaken, for example, for $(CdSe)_n$ for $n = 6$ by Liu et al.,[19a] $n = 1$−8 by Troparevsky et al.,[19b] $n = 3$, 6, 10, 13 by Chung et al.[20] and Kim et al.,[21] $n = 6$−54 by Nguyen et al.,[22] $n = 3$, 4, 6, 9 by Lim et al.,[23] $n = 6$, 9 by Kuznetsov et al.,[24] $n = 6$, 13 by Yang et al.,[25] $n = 33$,[26−28] $n = 13$, 19, 33 by Del Ben et al.,[29] n up to 16,[20,30−34] $n = 33$, 34,[10,35] and also for larger clusters.[36−38] Similarly, $(ZnS)_n$ SNCs were investigated theoretically regarding structure, optical excitations, and effects of ligands by Aspiroz et al.[39] and Malloci et al.[40] for $n = 6$, as well as for other cluster sizes.[40−48] Reliable prediction of the optical excitations requires

Received: March 11, 2013
Published: June 13, 2013

 © 2013 American Chemical Society dx.doi.org/10.1021/ct4001944 | J. Chem. Theory Comput. 2013, 9, 3581−3596

first prediction of the morphology because a bulklike structure cannot be assumed for ultrasmall SCNs. Previous studies were carried out at various levels of theory and were not fully benchmarked at high levels of theory, which is important in this case because of the difficulty in comparing to experimental spectra. Indeed, one of the main challenges in studying SNCs is structure determination, which involves locating the lowest-energy (LE) isomers or global minima among the larger number of possible isomers with increasing cluster size. With a suitable functional, density functional theory (DFT) provides an effective tool at low computational cost for structure prediction. However, systematic benchmark calculations to assess functionals for evaluating energies in ground and excited states have not been reported.

In this work, due to the lack of experimental and accurate computed results, a systematic study for the ground and excited states of small ZnS and CdSe clusters was first carried out to provide DFT functional performance benchmarks. We evaluated the accuracy of DFT functionals using the mean absolute errors (MAE) and mean signed errors (MSE) relative to benchmark coupled cluster (CC) method with singles, doubles (CCSD) and noniterative triples (CCSD(T)),[49] and the second order approximate CC (CC2)[50] methods. The accurate but computationally demanding results provided benchmarks for evaluating the applicability of the more economical DFT and time-dependent DFT (TDDFT) with different functionals for the ground and excited states, respectively. Use of the popular B3LYP demonstrated poor agreement with high-level ab initio results for the ground and excited state, although this functional has been used in a number of previous studies,[20,21,24−26,30−33,42−44] including our previous work for $(CdSe)_n$ clusters.[22] Next, structures and ground state spectra were reexamined for CdSe SNCs ranging in size from less than 1 nm to more than 2 nm using the PBE0 hybrid functional. This functional was shown in our benchmarking to provide a good description for both the ground and excited states for small clusters. Systematic passivation of bare clusters was also examined and compared with recent experimental data of one-photon absorption (OPA) spectra,[11,12] which has not been carried out for small $(CdSe)_n$ clusters. The results shed light into the influence of size, shape, and ligands on spectral properties of SNCs. $(ZnS)_n$ and $(CdSe)_n$ clusters with $n \geq 24$ possess clear wurtzite cores that may serve as basic units for transition to nanorods and bulklike wurtzite structures.

The paper is organized as follows. Section 2 provides computational details. Section 3 presents results and discussion for the benchmarking of ground state structures and energies in section A.1. and of excited states for the ligand-free and ligated clusters in section A.2. Section B.1 summarizes results and discussion of structure and energies of ZnS and CdSe clusters using the PBE0 functional. Section B.2 presents one-photon absorption spectra in comparison to available experimental data. Section 4 summarizes the findings and concludes the paper.

2. COMPUTATIONAL METHODS

Electronic structure calculations were done using the cc-pVTZ[51,52] basis set and a smaller version without *g* functions for Zn and Cd atoms, without *f* functions for Se, S C, N, and O atoms, and without *d* functions for hydrogen atoms. For $n = 3-6$, CCSD(T) values are obtained using basis set additivity correction at the MP2/cc-pVTZ structure as E[CCSD(T)] = E[CCSD(T)/SDD-6-31G*] + E(MP2/cc-pVTZ) − E(MP2/SDD-6-31G*). For CdSe clusters, we used the Stuttgart/Dresden effective core potentials and the correlated consistent valence triple-ζ basis set (cc-pVTZ-SD) of Martin and Sundermann.[52] CCSD(T) relative energies compared to different functionals are given in Table 1S of the Supporting Information. Excited states calculations were done using the completely renormalized equation-of-motion (CR-EOM) CCSD with noniterative triples correction (IA)[49] and second order approximate CC (CC2),[50] as implemented in the NWChem[53] program. Basis set effects and deviations obtained for CC2 compared to CCSD(T) values were found to be small. For CR-EOMCCSD(T), the MAE of 0.03 eV for using the smaller version of the cc-pVTZ basis set was obtained for the first 10 excited states of $(ZnS)_2$ (Table 2S of the Supporting Information). Thus, the compact version of the cc-pVTZ basis set was applied for larger clusters.

Kohn−Sham (KS)[54] DFT with B3LYP, CA-B3LYP, CAM-B3LYP, ωB97X, PBE0, PBE, BP86, PW91, and M06 was performed using the Gaussian 09 program.[55] Calculations for other long-range corrected functionals were carried out with a locally modified version of the GAMESS program[56] (see a description of the various functionals in ref 57). Effects of hydration/ligation were modeled by successively adding water and amines molecules to metallic and nonmetallic sites of the bare clusters to form a first solvation shell. To account for bulk solvent effects for the ligated clusters, TDDFT calculations were done using the nonequilibrium polarizable continuum model (PCM)[58,59] with the united atom cavity as previously described.[60]

Starting points for geometry optimization with various functionals were B3LYP structures that were determined by isomer enumeration and Monte Carlo basin hopping, as described in our previous work.[22] $(CdSe)_n$ topological motifs considered include Euler structures with all possible trivalent polyhedra (cages) having 4- and 6-atom rings, structures that are formed by polyhedra with cavities of concentrically confined smaller structures (cage−core or core−shell), and different hexagonal stacks that are made up to mimic the wurtzite bulklike crystal structure. The latter also includes a wurtzite lattice[28,29,38] constructed for $n = 13$, 19, and 33.

For $(ZnS)_n$ and $(CdSe)_n$ with $n > 6$, Stuttgart/Dresden (SD) valence basis set and ECP used for Zn, (8s7p6d)/[6s5p3d], Cd, (7s7p5d)/[5s5p2d], and Se, (4s5p2d)/[2s2p2d], includes two additional sets of d-functions for Se (ζ = 0.475412, 0.207776) atoms for better structures and energetics.[52,61−63] Additional polarization functions for atoms with high coordination in the cluster were previously[22,31] found important. Other atoms were treated with the 6-31G(d) basis set.[64,65] For selected cases, calculations were carried out using the larger correlated consistent valence triple-ζ basis set. The effects of basis sets were found to be small. The PBE0/SD-6-31G* results are discussed throughout, unless mentioned otherwise. For $n \leq 37$, the low-energy structures were verified to be minima on the potential energy surface by harmonic frequency calculations using the Gaussians 09 program.[55] TDDFT excitation energies and oscillator strengths were calculated using the Gaussian 09[55] and GAMESS[56] programs.

3. RESULTS AND DISCUSSION

A.1. Benchmarking of Ground State Structures and Energies. *Bare Clusters.* Structures and CCSD(T) relative (to the LE isomer) energies of the isomers of small $(ZnS)_n$ and

$(CdSe)_n$ (n = 2, 3, 4, 5, 6) clusters are shown in Figure 1. The LE structures for n = 2−4 are planar. The cage structure of

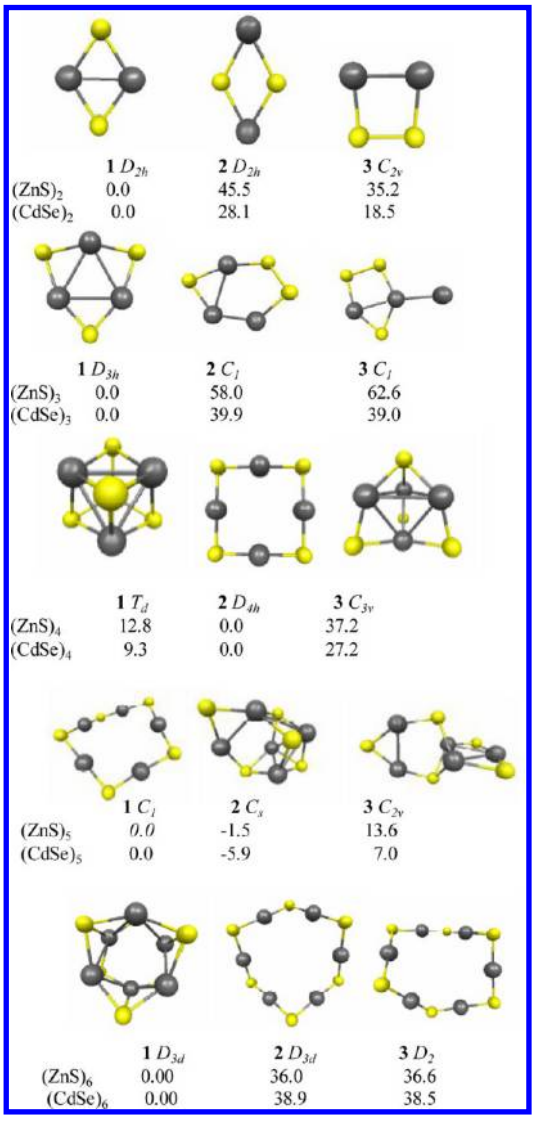

Figure 1. Structures and CCSD(T) relative energies for $(CdSe)_n$ and $(ZnS)_n$ isomers. Zn and Cd atoms are shown in black.

$(ZnS)_4$ with T_d symmetry is not the lowest energy structure as predicted by Matxain et al.[48] However, due to strong basis dependency, previous calculations using the BP86 functional and SVP basis set reported the T_d structure to be the global minimum for $(ZnS)_4$.[34] For $(ZnS)_5$, there are two nearly isoenergetic isomers. At the highest level of theory, the ten-membered ring is predicted to be slightly higher in energy. All methods predict for $(ZnS)_6$ and $(CdSe)_6$ to have a stack of two six-membered rings with D_{3d} symmetry, in agreement with previous studies.[20,24,32,33,43] Structures with a twelve-atom-ring are well separated in energy.

The MAEs for the relative energies of different functionals compared to the benchmark CCSD(T) values are given in Figure 2 for $(ZnS)_n$ and $(CdSe)_n$. The numerical values are tabulated in the Supporting Information (Table 1S). The MP2 results are within 5 kcal/mol of the CCSD(T) values. We note that functional performance varies significantly with cluster sizes. For a given cluster, the hybrid functionals appear to be better than GGAs, except for B3LYP. The large fluctuations

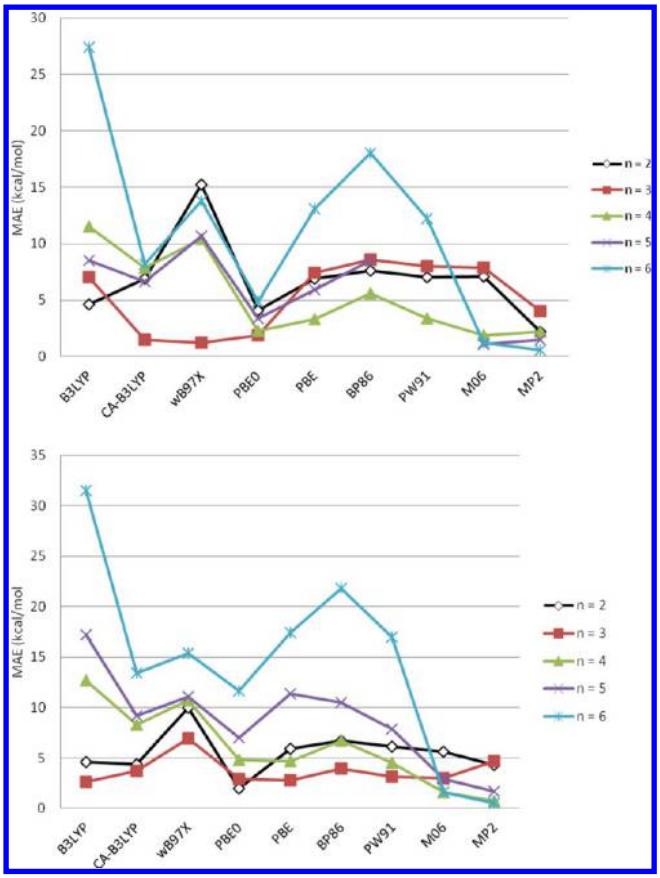

Figure 2. (top) $(ZnS)_n$ and (bottom) $(CdSe)_n$ mean absolute errors (MAEs) for relative energies (see Supporting Information Table 1S) compared to CCSD(T) for different functionals. CCSD(T) calculations were done using basis additivity correction at the MP2/cc-pVTZ structure: E[CCSD(T)] = E[CCSD(T)/SDD-6-31G*] + E(MP2/cc-pVTZ) − E(MP2/SDD-6-31G*).

and errors obtained with B3LYP are significantly reduced by CA-B3LYP and to the lesser extent by ωB97X, although both functionals include long-range HF exchange interactions. However, PBE0 and M06 appear to provide the best overall performance for ZnS and CdSe clusters, respectively. For $(ZnS)_6$ and $(CdSe)_6$, PBE0, B3LYP, and GGA functionals failed to predict the large energy gaps between the cage and twelve-atom-ring structures, leading to large MAEs (1.7−31.5 kcal/mol for $(CdSe)_6$, 4.9−27.2 kcal/mol for $(ZnS)_6$). M06 has the lowest errors for n = 6, with MAEs of 1.2 and 2.6 kcal/mol for $(ZnS)_6$ and $(CdSe)_6$, respectively.

Hydrated Clusters. Structures and relative energies for hydrated clusters are shown in Figure 3. Two water molecules were found to preferably bind at metallic sites to form two nearly isoenergetic structures for $(ZnS)_2$−$2H_2O$ while the water-dimer (W2) coordination was the most stable structure for $(CdSe)_2$−$2H_2O$. For four water molecules, the additional waters can form oxygen−metallic bonds or hydrogen bonds at nonmetallic sites and the coordinated waters. The latter W2 configurations were found to be more stable for n = 2 (Figure 3a). The former structure (**e**) lies about 10 kcal/mol higher in energy, which is slightly reduced after zero-point energy (by 1 kcal/mol) corrections. Tetra-coordinated clusters have two waters per metal atom. Clusters with 12 waters appear to fully form a first solvation shell. Hydration for n = 3 (Figure 3b) follows a similar coordination patterns with W2 coordination

dx.doi.org/10.1021/ct4001944 | J. Chem. Theory Comput. 2013, 9, 3581−3596

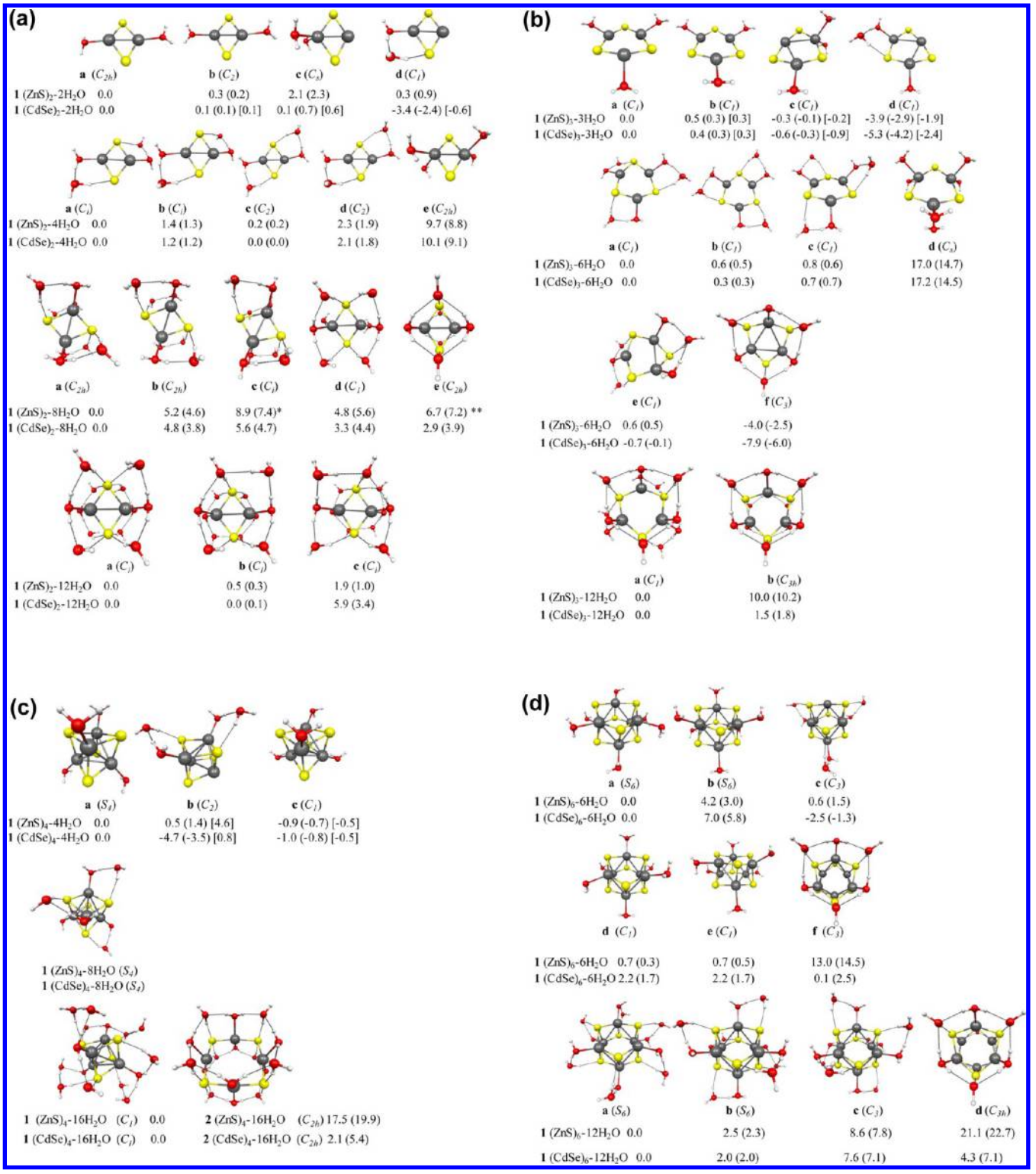

Figure 3. (a) PBE0/cc-pVTZ hydrated $(AB)_2$ structures and relative energies (in kilocalories per mole). Values in parentheses and brackets are PBE0 and MP2 zero-point corrected energies, respectively. Structures with one (*) and two (**) imaginary frequencies. (b) PBE0/cc-pVTZ hydrated $(AB)_3$ structures and relative energies (in kilocalories per mole).Values in parentheses and brackets are PBE0 and MP2 zero-point corrected energies, respectively. (c) PBE0/cc-pVTZ hydrated $(AB)_4$ structures and relative energies (in kilocalories per mole). Values in parentheses and brackets are PBE0 and MP2 zero-point corrected energies, respectively. (d) PBE0/cc-pVTZ hydrated $(AB)_6$ structures and relative energies (in kilocalories per mole). Values in parentheses are zero-point corrected energies.

with three waters. For six waters, the W2 hydrated structure (**a**) is more than 10 kcal/mol lower in energy than the metal hydrated (d) structure (Figure 3b). However, the trimer-coordinated (W3) and hexamer-coordinated (W6) are also competitive. The latter (structure **f**) appears to be the most stable. Thus, tetra-coordinated clusters for $n = 3$ can form a two-hexamer-coordinated structure with twelve waters. However, the distorted structures with one water-hexamer are more

dx.doi.org/10.1021/ct4001944 | J. Chem. Theory Comput. 2013, 9, 3581−3596

Table 1. Comparison of cc-pVTZ S_0-S_n Excitation Energy (E, in Electronvolts) and Oscillator Strength (f)

1 (D_{2h}) $(ZnS)_2$									**1** (C_{2h}) $(ZnS)_2-2H_2O$								
	PBE0		CAM		CA		CC2	CC		PBE0		CAM		CA		CC2	CC[b]
state[a]	E	f	E	f	E	f	E	E	state	E	f	E	f	E	f	E	E
$^1B_{2g}$	2.17		2.27		1.88		2.13	2.15	^1B_g	3.14		3.29		3.45		3.45	3.47
$^1B_{1u}$	2.87	0.01	2.94	0.01	2.59	0.01	2.79	2.88	^1A_u	3.70	0.02	3.82	0.02	3.97	0.03	3.99	4.08
$^1B_{3u}$	3.12	0.02	3.28	0.03	2.80	0.02	3.23	3.24	^1A_u	3.86	0.00	4.19	0.00	4.27	0.00	4.48	4.47
MAE	0.05		0.07		0.33		0.04			0.44		0.24		0.11		0.04	
MSE	−0.04		0.07		−0.33		−0.04			−0.44		−0.24		−0.11		−0.03	

1a (C_i) $(ZnS)_2-4H_2O$					**1a** (C_{2h}) $(ZnS)_2-8H_2O$					**1a** (C_i) $(ZnS)_2-12H_2O$			
	PBE0		PBE0-PCM			PBE0		PBE0-PCM			PBE0		PBE0-PCM	
state[a]	E	f	E	f	state	E	f	E	f	state	E	f	E	f
^1A_g	3.90		4.47		^1B_g	4.81		5.02		^1A_g	5.39		5.36	
^1A_u	4.31	0.04	4.80	0.09	^1B_u	4.83	0.06	5.12	0.10	^1A_u	5.41	0.11	5.44	0.14
^1A_u	4.66	0.02	5.15	0.13	^1A_u	5.22	0.16	5.38	0.20	^1A_u	5.66	0.21	5.62	0.22

1 (D_{2h}) $(CdSe)_2$									**1** (C_{2h}) $(CdSe)_2$-$2H_2O$							
	PBE0		CAM		CA		CC2	CC		PBE0		CAM		CA		CC2
state[c]	E	f	E	f	E	f	E	E	state	E	f	E	f	E	f	E
$^1B_{2g}$	1.70		1.85		1.74		1.53	1.70	^1B_g	2.43		2.67		2.55		2.50
$^1B_{1u}$	2.52	0.02	2.57	0.02	2.49	0.02	2.24	2.42	^1A_u	3.08	0.00	3.30	0.04	3.21	0.04	3.11
$^1B_{3u}$	2.37	0.02	2.57	0.02	2.49	0.02	2.30	2.45	^1B_u	3.11	0.04	3.40	0.06	3.30	0.06	3.30
MAE	0.06		0.14		0.05		0.17			0.10		0.15		0.05		
MSE	0.01		0.14		0.05		−0.17			−0.10		0.15		0.05		

1a (C_i) $(CdSe)_2-4H_2O$					**1a** (C_{2h}) $(CdSe)_2-8H_2O$					**1a** (C_i) $(CdSe)_2-12H_2O$			
	PBE0		PBE0-PCM			PBE0		PBE0-PCM			PBE0		PBE0-PCM	
state[d]	E	f	E	f	state	E	f	E	f	state	E	f	E	f
^1A_g	2.91		3.49		^1B_g	3.75		3.90		^1A_g	4.22		4.17	
^1A_u	3.37	0.04	3.79	0.12	^1B_u	3.85	0.09	4.00	0.15	^1A_u	4.29	0.13	4.23	0.19
^1A_u	3.50	0.04	3.98	0.11	^1A_u	4.10	0.11	4.21	0.14	^1A_u	4.46	0.12	4.40	0.15

[a]Using cc-pVTZ without g functions for Zn, f functions for S, at the PBE0/cc-pVTZ geometry. [b]Using cc-pVTZ without g functions for Zn, f functions for S, at the MP2/cc-pVTZ geometry. [c]Using cc-pVTZ-SD without g functions for Cd, f functions for Se, using MP2/cc-pVTZ-SD geometry. [d]Using cc-pVTZ-SD without g functions for Cd, f functions for Se, using PBE0/cc-pVTZ-SD geometry.

stable for $(ZnS)_3-12H_2O$ and $(CdSe)_3-12H_2O$. For n = 4 (Figure 3c), the tetra-hydrated cubic cage was found to be more stable than the corresponding eight-membered-ring. However, the energy difference between the two structures narrows with sixteen waters. W2-hydration with two uncoordinated metallic sites was found to be the most stable for $(CdSe)_4$ with four waters. This is also true for $(CdSe)_6$ with three (c) and six (a) W2-hydrated sites for six- and twelve-water coordinations, respectively (Figure 3d). The W6-coordinations do not appear to be competitive in energy for $(CdSe)_6$ and $(ZnS)_6$. In comparison to previous optimization work[42] for $(ZnS)_6-6H_2O$, the reported C_1 structures appears to be similar to isomer **e** in Figure 3. Other low-lying structures were not reported. PBE0 predicts the lowest (classical or zero-point corrected) energy structure (**a**) to possess S_6 symmetry. However, there are three other structures (**c**, **d**, **e**) lying within 1 kcal/mol in energy on potential energy surfaces of $(ZnS)_6-6H_2O$. For $(CdSe)_6-6H_2O$, W2-hydration at three metallic sites is the most stable for the $(CdSe)_6$ cage with six waters (**c**).

A.2. Benchmarking of Excited States. *Bare Clusters.* The TDDFT with PBE0, CAM-B3LYP (labeled as CAM), and CA-B3LYP (labeled as CA) and CC2 results for the three lowest excited states of the bare clusters are shown in Tables 1−4 along with the calculated values for the hydrated clusters. Values obtained with CR-CCSD(T)/IA (labeled as CC) are also included for some clusters. The calculated values for other functionals and higher excited states are given in the Supporting Information (Table 2S and 3S). Red shifts are generally observed for the first transition band as the cluster increases in size. However, the first excited states drastically increase going from n = 2 to n = 3. CC2 predicted blue-shifts of 1.78 and 1.62 eV for ZnS and CdSe clusters, respectively. In contrast, increasing the cluster size from n = 3 to n = 4 does not result in significant changes in the excitation energies for the first excited states, specifically in blue-shifts of 0.03 and 0.12 eV for ZnS and CdSe clusters, respectively. Note that using the T_d structures as references results in large red-shifts (0.70, 0.79 eV for ZnS and CdSe clusters, respectively), leading to the small blue-shifts (0.2−0.3 eV) for going from n = 4 to n = 6. However, the T_d cages are not the lowest energy structures for $(ZnS)_4$ and $(CdSe)_4$ clusters (see Figure 1). Thus, the first excited states red-shift (0.44 eV for ZnS, 0.69 eV for CdSe) upon going from the lowest energy structures (D_{4h} for ZnS, D_{2d} for CdSe) for n = 4 to n = 6 (D_{3d}). Note that the first excited states of these clusters are weak in intensity or nonallowed transitions. Their energy levels and intensities are strongly perturbed by ligands/solvents.

The MAEs for excitation energies using TDDFT are summarized in Figures 4 and 5 for PBE0, M06, B3LYP, CAM-B3LYP, and CA-B3LYP. The CR-EOMCCSD(T) reference values were used for small clusters (n = 2−3) while CC2 values were used other clusters. CC2 MAEs of 0.04−0.05 eV were obtained for all systems, except for $(CdSe)_2$ with a MAE of 0.10 eV. For $(ZnS)_4$ and $(ZnS)_6$, our reference CC2

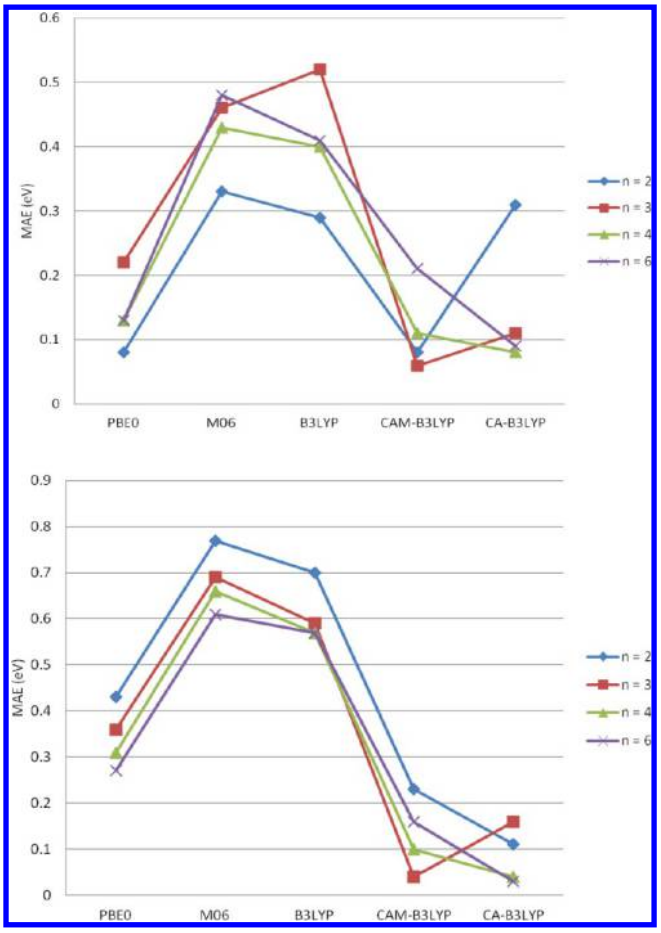

Figure 4. (top) Bare and (bottom) hydrated $(ZnS)_n$ mean absolute errors (MAEs) for excitation energies compared to CCSD(T)/CC2 for different functionals.

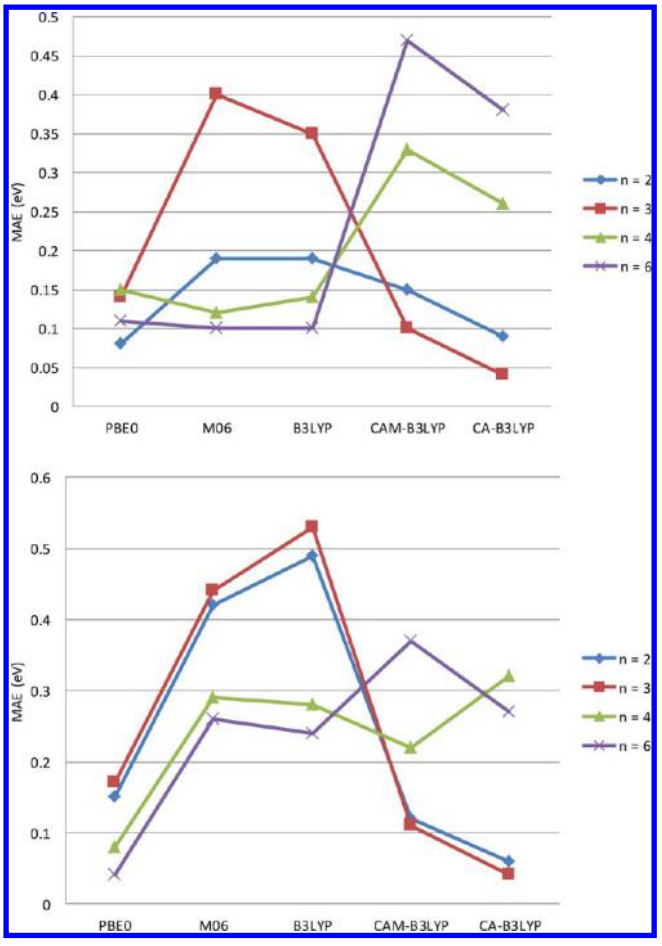

Figure 5. (top) Bare and (bottom) hydrated $(CdSe)_n$ mean absolute errors (MAEs) for excitation energies compared to CCSD(T)/CC2 for different functionals.

values for the first and second excitation energies are in good agreement with the CC2 and CASPT2 values reported recently.[43] The higher excited states CASPT2 energies reported[43] for $(ZnS)_4$ are comparable to the corresponding B3LYP values. For the bare $(ZnS)_n$ clusters, TDDFT with the hybrid PBE0 and the long-range hybrid CAM-B3LYP were found to have the smallest MAEs of about 0.1−0.2 eV, much smaller than the errors of about 0.3−0.5 eV obtained with other functionals. The CAM-B3LYP overestimates the excitation energies for $(ZnS)_6$, and the MAE of 0.21 eV is particularly large in comparison with smaller clusters. This is also true for $(CdSe)_6$. However, the MAE of 0.47 eV is significantly larger. In contrast, the PBE0, B3LYP, and M06 functionals show a clear improvement over the CAM-B3LYP and CA-B3LYP functionals (see Figure 5). For CdSe clusters, the overall MAEs of 0.1−0.2 eV obtained with PBE0 appear to be most consistent. The errors obtained with other functionals vary more widely with cluster size (see Figure 5). For example, the predicted CAM-B3LYP (MAEs of 0.10−0.15 eV) and CA-B3LYP (MAEs of 0.04−0.09 eV) values are in good agreement with the CC2 results for the small $(CdSe)_2$ and $(CdSe)_3$ clusters. However, for the larger cages of $(CdSe)_4$ and $(CdSe)_6$, the MAEs increase to 0.33−0.47 eV for CAM-B3LYP and 0.26−0.38 eV for CA-B3LYP. In contrast, the errors obtained with M06 and B3LYP $(CdSe)_4$ and $(CdSe)_6$ are small (~0.1 eV) compared to smaller clusters. Thus, consistent good agreements obtained with PBE0 in comparison with the CC2 and CCSD(T) results for the bare and hydrated (as shown below) CdSe clusters led us to select the functional to treat larger size clusters.

Hydrated Clusters. The effects of hydration on OPA were examined by ligated clusters, produced by successively adding water molecules to metallic and nonmetallic sites of the lowest-energy bare clusters to form a first solvation shell. To account for bulk solvent effects, excited state calculations for the ligated clusters were done using the TDDFT-PCM method. As previously done for the bare clusters, the coupled-cluster results for hydrated $(ZnS{-}H_2O)_n$ and $(CdSe{-}H_2O)_n$ (n = 2−4 and 6) clusters were used to evaluate the quality of functionals for TDDFT, as summarized by overall MAEs in Figures 4 and 5. The results for selected functionals for the three lowest excited states of the hydrated clusters are listed in Tables 2−4 along with values for the anhydrous counter parts. Values obtained with other functionals and higher excited states are listed in Tables 4S and 5S in the Supporting Information.

Hydration blue-shifts excitation energies and increases oscillator strengths for ZnS and CdSe clusters. The blue-shifts in excitation energies for the hydrated clusters can be attributed to the destabilization of virtual molecular orbitals (MOs) and to a lesser extent, the occupied MOs, due to the electron-donating nature of the oxygen atoms in the coordinating water molecules. The lowest unoccupied MOs of hydrated clusters are generally more delocalized due to significant contributions from water molecules (Supporting Information Figures 4S and

dx.doi.org/10.1021/ct4001944 | J. Chem. Theory Comput. 2013, 9, 3581−3596

Table 2. Comparison of cc-pVTZ S_0-S_n Excitation Energy (E, in Electronvolts) and Oscillator Strength (f)

1 (D_{3h}) $(ZnS)_3$									**1** (C_s) $(ZnS)_3-6H_2O$							
	PBE0		CAM		CA		CC2	CC		PBE0		CAM		CA		CC2
state[a]	E	f	E	f	E	f	E	E	state	E	f	E	f	E	f	E
$^1E''$	3.72		3.93		3.79		3.91	3.93	$^1A''$	4.26	0.00	4.61	0.00	4.46	0.00	4.60
$^1A_2''$	4.52	0.04	4.74	0.06	4.62	0.06	4.84	4.79	$^1A''$	4.27	0.00	4.61	0.00	4.46	0.00	4.60
$^1E'$	4.74	0.01	4.93	0.02	4.80	0.02	4.94	4.93	$^1A''$	4.82	0.23	5.17	0.34	5.03	0.34	5.24
MAE	0.22		0.02		0.15		0.03			0.36		0.03		0.16		
MSE	−0.22		−0.02		−0.15		0.01			−0.36		−0.02		−0.16		

1a (C_1) $(ZnS)_3-3H_2O$					**1a** (C_1) $(ZnS)_3-6H_2O$					**1a** (C_1) $(ZnS)_3-12H_2O$			
	PBE0		PBE0-PCM			PBE0		PBE0-PCM			PBE0		PBE0-PCM	
state[b]	E	f	E	f	state	E	f	E	f	state	E	f	E	f
^1A	4.26	0.00	4.65	0.00	^1A	4.68	0.00	4.87	0.00	^1A	5.07	0.04	5.18	0.05
^1A	4.27	0.00	4.65	0.00	^1A	4.69	0.00	4.88	0.01	^1A	5.07	0.04	5.18	0.05
^1A	4.95	0.13	5.26	0.21	^1A	5.25	0.15	5.37	0.23	^1A	5.45	0.19	5.52	0.23

1 (D_{3h}) $(CdSe)_3$									**1d** (C_s) $(CdSe)_3-6H_2O$							
	PBE0		CAM		CA		CC2	CC		PBE0		CAM		CA		CC2
state[c]	E	f	E	f	E	f	E	E	state	E	f	E	f	E	f	E
$^1E''$	3.11		3.34		3.24		3.15	3.24	$^1A''$	3.57	0.00	3.85	0.00	3.75	0.00	3.71
$^1A_2''$	3.73	0.05	3.94	0.07	3.84	0.07	3.85	3.88	$^1A''$	3.57	0.00	3.85	0.00	3.75	0.00	3.71
$^1E''$	3.76		4.04		3.96		3.92	3.94	$^1A''$	4.03	0.16	4.30	0.23	4.20	0.24	4.25
MAE	0.15		0.09		0.02		0.05			0.17		0.11		0.04		
MSE	−0.15		0.09		−0.01		−0.05			−0.17		0.11		0.01		

1a (C_1) $(CdSe)_3-3H_2O$					**1a** (C_1) $(CdSe)_3-6H_2O$					**1a** (C_1) $(CdSe)_3-12H_2O$			
	PBE0		PBE0-PCM			PBE0		PBE0-PCM			PBE0		PBE0-PCM	
state[d]	E	f	E	f	state	E	f	E	f	state	E	f	E	f
^1A	3.38	0.00	3.71	0.00	^1A	3.69	0.00	3.90	0.00	^1A	4.07	0.02	4.12	0.03
^1A	3.43	0.00	3.72	0.00	^1A	3.71	0.00	3.92	0.01	^1A	4.07	0.02	4.13	0.03
^1A	3.96	0.11	4.19	0.19	^1A	4.14	0.10	4.30	0.19	^1A	4.38	0.12	4.42	0.18

[a]Using cc-pVTZ without g functions for Zn, f functions for S, at the MP2/cc-pVTZ geometry. [b]Using cc-pVTZ without g functions for Zn, f functions for S, at the PBE0/cc-pVTZ geometry. [c]Using cc-pVTZ without g functions for Zn, f functions for S, at the MP2/cc-pVTZ geometry. [d]Using cc-pVTZ-SD without g functions for Cd, f functions for Se, using PBE0/cc-pVTZ-SD geometry.

5S). The increase in intensity for transitions in the hydrated clusters compared to bare clusters can be ascribed to the delocalization nature of the orbitals involved in the excitations. For a given cluster size, the blue-shifts are generally larger for $(ZnS)_n$ compared to $(CdSe)_n$. Errors obtained for the hydrated CdSe clusters are generally smaller than the deviations found for the ligated ZnS counterparts (cf. Figures 4 and 5). For $(ZnS-H_2O)_6$, the allowed band previously[42] predicted by B3LYP to occur at slightly above 4 eV is in good agreement with our calculated value of 4.07 eV for the first allowed transition (Supporting Information Table 4S). However, B3LYP significantly underestimates the excitation energies for $(ZnS-H_2O)_6$ (0.61 eV on average); and errors progressively increase for smaller hydrated clusters. Interestingly, the errors obtained with CAM-B3LYP are not significantly different from corresponding anhydrous clusters. Except for $(ZnS)_3$, the CA-B3LYP errors for hydrated ZnS clusters are slightly improved compared to the anhydrous values. However, larger errors are obtained for hydrated clusters using other functionals. The largest MAEs of about 0.7−0.8 eV are obtained with B3LYP and M06 functionals for $(ZnS)_2-2H_2O$ and $(ZnS)_2-4H_2O$ (see Figure 4 and Table 4S of the Supporting Information). For PBE0, the errors are slightly reduced (0.4−0.5 eV) and decrease with increasing cluster size. This is also true for hydrated $(CdSe)_n$ with n = 3−6). The errors obtained with PBE0 for hydrated CdSe clusters are comparable to corresponding anhydrous clusters in MAEs. However, the predicted PBE0 excitation energies for hydrated CdSe cluster are generally underestimated. PBE0 excitation energies are generally higher than the B3LYP values due to the HF exchange and GGA part of the functionals acting upon excitation energy. Increasing amount of HF exchange, which is important for proper treatments of systems with CT character, generally increases the predicted excitation energies. The excitation energies using the PBE exchange-correlation functional are typically higher than the corresponding BLYP values and similarly upon increasing the amount of HF exchange. As shown in Table 4S, a 5% increase in HF exchange in PBE0 results in an average increase of about 0.2 eV in excitation energies for $(ZnS-2H_2O)_4$ and $(ZnS-H_2O)_6$. About the same amount of difference in excitation energies was obtained with BLYP in comparison to PBE for the two hydrated systems.

As predicted by CC2, adding one water molecule to each metallic site of $(ZnS)_n$ blue-shifts the first excited state by about 1.32, 1.15, and 1.09 eV for n = 2, 4, 6, respectively. The corresponding shifts for $(CdSe)_n$ are smaller (0.97, 0.92, and 0.76 eV for n = 2, 4, 6, respectively). The TDDFT predicted shifts are in good agreement with the CC2 values for hydrated $(CdSe)_n$ and the larger size $(ZnS)_n$ clusters. TDDFT using the PBE0 functional, for example, underestimates the CC2 shifts by about 0.2 eV for the hydrated $(CdSe)_n$, but the errors for

Table 3. Comparison of cc-pVTZ S_0-S_n Excitation Energy (E, in Electronvolts), Oscillator Strength (f)

1 (T_d) $(ZnS)_4$								**1** (S_4) $(ZnS)_4-4H_2O$							
	PBE0		CAM		CA		CC2[b]		PBE0		CAM		CA		CC2
state[a]	E	f	E	f	E	f	E	state	E	f	E	f	E	f	E
$^1T_1$	3.26		3.45		3.32		3.21	^1E	4.11	0.06	4.49	0.08	4.34	0.07	4.36
$^1T_2$	3.35	0.03	3.58	0.03	3.44	0.03	3.31	^1A	4.21	0.00	4.58	0.00	4.43	0.00	4.47
^1E	4.52		4.68		4.60		4.66	^1E	4.22	0.01	4.59	0.01	4.44	0.01	4.48
MAE	0.08		0.18		0.10				0.26		0.12		0.03		
MSE	−0.02		0.18		0.06				−0.26		0.12		−0.03		

1a (C_1) $(ZnS)_4-4H_2O$					**1a** (S_4) $(ZnS)_4-8H_2O$					**1a** (C_1) $(ZnS)_4-16H_2O$				
	PBE0		PBE0-PCM			PBE0		PBE0-PCM			PBE0		PBE0-PCM	
state[c]	E	f	E	f	State	E	f	E	f	State	E	f	E	f
^1A	4.26	0.07	4.57	0.07	^1E	4.69	0.08	4.93	0.14	^1A	5.19	0.14	5.21	0.20
^1A	4.29	0.07	4.63	0.08	^1E	4.82	0.02	5.04	0.02	^1A	5.19	0.14	5.21	0.20
^1A	4.32	0.07	4.66	0.03	^1A	4.82	0.00	5.01	0.00	^1A	5.29	0.18	5.29	0.22

2 (D_{4h}) $(ZnS)_4$								**2** (D_{2d}) $(CdSe)_4$							
	PBE0		CAM		CA		CC2		PBE0		CAM		CA		CC2
state[d]	E	f	E	f	E	f	E	state	E	f	E	f	E	f	E
$^1B_{1u}$	3.68	0.00	4.03	0.00	3.91	0.00	3.94	$^1A_1$	3.16		3.49		3.42		3.27
$^1B_{1u}$	4.19	0.00	4.46	0.00	4.33	0.00	4.40	^1E	3.48	0.00	3.80	0.00	3.74	0.00	3.64
^1E_g	4.19		4.56		4.46		4.57	$^1A_1$	3.53		3.80		3.70		3.65
MAE	0.28		0.05		0.07				0.13		0.18		0.10		
MSE	−0.28		0.05		−0.07				−0.13		0.18		0.10		

1 (T_d) $(CdSe)_4$								**1** (S_4) $(CdSe)_4-4H_2O$							
	PBE0		CAM		CA		CC2		PBE0		CAM		CA		CC2
state[d]	E	f	E	f	E	f	E	state	E	f	E	f	E	f	E
$^1T_1$	2.66		2.85		2.75		2.36	^1E	3.34	0.06	3.54	0.06	3.65	0.06	3.28
$^1T_2$	2.78	0.04	3.01	0.05	2.90	0.05	2.49	^1A	3.39	0.00	3.58	0.00	3.69	0.00	3.34
^1E	3.63		3.76		3.71		3.54	^1E	3.43	0.03	3.62	0.06	3.73	0.06	3.38
MAE	0.23		0.41		0.32				0.05		0.25		0.36		
MSE	0.23		0.41		0.32				0.05		0.25		0.36		

1a (C_1) $(CdSe)_4-4H_2O$					**1a** (S_4) $(CdSe)_4-8H_2O$					**1a** (S_4) $(CdSe)_4-16H_2O$				
	PBE0		PBE0-PCM			PBE0		PBE0-PCM			PBE0		PBE0-PCM	
state[e]	E	f	E	f	state	E	f	E	f	state	E	f	E	f
^1A	3.37	0.05	3.55	0.09	^1E	3.64	0.07	3.76	0.14	^1E	4.01	0.13	3.94	0.20
^1A	3.41	0.07	3.60	0.07	^1E	3.72	0.05	3.81	0.06	^1E	4.10	0.02	4.02	0.02
^1A	3.42	0.01	3.62	0.11	^1A	3.72	0.00	3.81	0.00	^1A	4.10	0.00	4.03	0.00

[a]Using cc-pVTZ without g functions for Zn, f functions for S, at the MP2/cc-pVTZ geometry. [b]CC2: 3.13, 3.21. CASPT2: 3.01, 3.22 (f = 0.04), 4.32. Ref 43. [c]Using cc-pVTZ without g functions for Zn, f functions for S, at the PBE0/cc-pVTZ geometry. [d]Using cc-pVTZ-SD without g functions for Cd, f functions for Se, using PBE0/cc-pVTZ-SD geometry. [e]Using cc-pVTZ-SD without g functions for Zn, f functions for S, using PBE0/cc-pVTZ-SD geometry.

$(ZnS)_n$ vary from 0.35, 0.30, and 0.16 eV for n = 2, 4, 6, respectively. Further blue-shifts are observed by including ligating waters at nonmetallic sites and the bulk hydrating effects with PCM. However, the effects from PCM are diminished for hydrated clusters with a fully formed first solvation shell. For $(ZnS)_2$ and $(CdSe)_2$ with 12 ligating waters, the PBE0 first excited state are blue-shifted by about 3.2 and 2.5 eV, respectively. Intense transitions are predicted to occur in the range of about 4.2−4.6 and 4.4−4.6 eV, for $(CdSe)_2$ and $(CdSe)_3$ with 12 ligating waters, respectively (Tables 1 and 2). For the fully hydrated $(ZnS)_4$ and $(CdSe)_4$, the low-lying excited states obtained with TDDFT-PCM and PBE0 form the first OPA bands at about 5.2 and 4 eV, respectively (Table 3). Moving to the larger $(ZnS)_6$ and $(CdSe)_6$ clusters with 12 water molecules, the first allowed transitions reduce to about 4.9 and 3.7 eV (Table 4). For $(ZnS)_6-12H_2O$, the optimized structure is slightly distorted from S_6 symmetry to C_i symmetry. This results in two degenerate ^1A_g excited states corresponding to ^1E_g under S_6 symmetry. One of two degenerate ^1A_g states is included in the table. The observed aqueous and methanol colloidal spectra for 2 nm (in diameter) ZnS clusters showed the lowest transition of about 4.3 eV. Smaller ZnS clusters (prepared at −77 °C in methanol) were identified[15] by the absorption peaks at 228 nm (5.44 eV) and 243 nm (5.10 eV), which are in the range reported for other ligands[16,66−68] and predicted values for the hydrated clusters of $(ZnS)_4$ and $(ZnS)_6$. Experimentally prepared CdSe clusters with average diameters in the range of 2−5 nm in an aqueous colloidal mixture exhibited a lowest energy band at about 3.3 eV (~380 nm).[13]

B.1. Larger CdSe Clusters: Ground State Structures and Energies. Due to good agreement with high-level ab

dx.doi.org/10.1021/ct4001944 | J. Chem. Theory Comput. 2013, 9, 3581−3596

Table 4. Comparison of cc-pVTZ S_0-S_n Excitation Energy (E, in Electronvolts) and Oscillator Strength (f)

1(D_{3d}) $(ZnS)_6$								**1a** (S_6) $(ZnS)_6-6H_2O$							
	PBE0		CAM		CA		CC2[b]		PBE0		CAM		CA		CC2
state[a]	E	f	E	f	E	f	E	state	E	f	E	f	E	f	E
^1E_g	3.44		3.77		3.65	0.00	3.50	^1E_g	4.37		4.79		4.64		4.59
$^1A_{2u}$	3.71	0.02	4.06	0.03	3.94	0.03	3.81	^1A_u	4.41	0.09	4.85	0.14	4.69	0.14	4.66
^1E_g	4.26		4.61		4.48		4.41	^1E_g	5.04		5.48		5.32		5.33
MAE	0.10		0.24		0.12				0.25		0.18		0.03		
MSE	−0.10		0.24		0.12				−0.25		0.18		0.02		

1a (S_6) $(ZnS)_6-6H_2O$					**1c** (C_3) $(ZnS)_6-6H_2O$					**1a** (C_i) $(ZnS)_6-12H_2O$				
	PBE0		PBE0-PCM			PBE0		PBE0-PCM			PBE0		PBE0-PCM	
state[c]	E	f	E	f	state	E	f	E	f	state	E	f	E	f
^1E_g	4.39		4.58		^1E	3.92	0.01	4.42	0.01	^1A_g	4.69		4.84	
^1A_u	4.42	0.09	4.63	0.17	^1A	4.00	0.03	4.52	0.11	^1A_u	4.71	0.12	4.86	0.19
^1E_g	5.05		5.20		^1E	4.50	0.01	5.03	0.03	^1A_g	5.24		5.34	

1(D_{3d}) $(CdSe)_6$								**1a** (S_6) $(CdSe)_6-6H_2O$							
	PBE0		CAM		CA		CC2		PBE0		CAM		CA		CC2
state[d]	E	f	E	f	E	f	E	state	E	f	E	f	E	f	E
^1E_g	2.80		3.12		3.03		2.58	^1E_g	3.38		3.75		3.66		3.34
$^1A_{2u}$	3.08	0.03	3.42	0.05	3.33	0.05	2.90	^1A_u	3.51	0.11	3.91	0.19	3.81	0.19	3.48
^1E_g	3.45		3.82		3.74		3.32	^1E_u	4.08	0.02	4.39	0.01	4.28	0.01	4.12
MAE	0.18		0.52		0.43				0.04		0.37		0.27		
MSE	0.18		0.52		0.43				0.01		0.37		0.27		

1a (S_6) $(CdSe)_6-6H_2O$					**1c** (C_3) $(CdSe)_6-6H_2O$					**1a** (S_6) $(CdSe)_6-12H_2O$				
	PBE0		PBE0-PCM			PBE0		PBE0-PCM			PBE0		PBE0-PCM	
state[c]	E	f	E	f	state	E	f	E	f	state	E	f	E	f
^1E_g	3.34		3.43		^1E	3.09	0.00	3.38	0.00	^1E_g	3.50		3.56	
^1A_u	3.44	0.11	3.54	0.20	^1A	3.21	0.05	3.53	0.19	^1A_u	3.59	0.12	3.65	0.20
^1E_u	4.02	0.03	4.06	0.06	^1E	3.71	0.01	4.01	0.00	^1E_u	4.14	0.16	4.14	0.33

[a]Using cc-pVTZ without g functions for Zn, f functions for S, at the MP2/cc-pVTZ geometry. [b]MPW91: 3.37 (^1E_g), 3.60 ($^1A_{2u}$, f = 0.03).[48] CC2: 3.40 (^1E_g), 3.67 ($^1A_{2u}$). CASPT2: 3.29 (^1E_g), 3.44 ($^1A_{2u}$, f = 0.04).[43] [c]Using cc-pVTZ without g functions for Zn, f functions for S, at the PBE0/cc-pVTZ geometry. [d]Using cc-pVTZ-SD without g functions for Zn, f functions for S, using MP2/cc-pVTZ-SD geometry.

initio results for the ground and excited states obtained with PBE0 for small ZnS and CdSe clusters (vide supra), larger NPs are examined with the same hybrid functional. For the ground state relative energies, PBE0 has the lowest (2 kcal/mol) mean absolute error (MAE) for $(ZnS)_n$ for n = 7−24 (see Supporting Information Table 7S). The MAE for excitation energies obtained with PBE0 for the bare ZnS is well within the typical error of about 0.25 eV for valence excited states. Larger errors for $(ZnS-2H_2O)_2$ and $(ZnS-2H_2O)_3$ are obtained with PBE0; the errors for larger hydrated ZnS clusters are not out of the typical range. However, we note that PBE0 excitation energies for ZnS clusters are generally less accurate than the corresponding values for CdSe clusters. We found that systems varying degree of CT character require different amounts HF exchange. Thus, functionals such as CA-B3LYP that provide good estimates for modest CT transitions have significant errors for strong CT excitations. Functionals that provide accurate long-range CT excitation energies overestimate local or weak CT transitions. Thus, we clarify that no functional, including the CAM-B3LYP, was found to be the best for all systems considered.

Figure 6a and b summarizes the energies of different $(ZnS)_n$ and $(CdSe)_n$ motifs relative to the global minima for PBE0 compared to results using B3LYP, which favors cage over wurtzite and cage−core topologies. Bare clusters are predicted by PBE0 to assume the wurtzite motif for $(ZnS)_{21}$ and $(CdSe)_{20}$, while the B3LYP results show it to be the most stable for $(CdSe)_{34}$. Similarly, PBE0 generally predicts cage−core structures to be energetically more favorable for smaller clusters than the corresponding clusters obtained with B3LYP.

The relative stability (ΔE_n) for the lowest-energy (LE) clusters is calculated as

$$\Delta E_n = E_{n+1} + E_{n-1} - 2E_n \quad (1)$$

where E_n is the total energy of the SNC. A positive ΔE_n indicates that a cluster (n) is more stable than the larger (n + 1) cluster due to an endothermic driving force for incremental growth (n + 1) and decay (n − 1) of the cluster. ΔE_n for ZnS clusters are shown in Figure 6c, while the corresponding values for the bare and amine passivated CdSe clusters are given in Figure 6d. We note that passivation significantly shifts the cluster's relative stability and changes the lowest-energy structural motif for some clusters. In the following sections, we discuss first the results in more detail for ligand-free clusters and then the influence of ligands on the stability and spectra.

Bare Clusters. Laser ablation on binary group II−VI semiconductors (CdSe, CdS, CdTe, ZnS, and ZnSe) produced spectral peaks consistent with $(II-VI)_n$ clusters with n = 13, 19, 33, and 34.[10,32,36] However, experimental structures for these clusters have not been reported. Calculated $(ZnS)_n$ and $(CdSe)_n$ structures are given in Figure 7a and b. Relative energies of low energy local minima for $(ZnS)_n$ (n = 7−24) are

dx.doi.org/10.1021/ct4001944 | J. Chem. Theory Comput. 2013, 9, 3581−3596

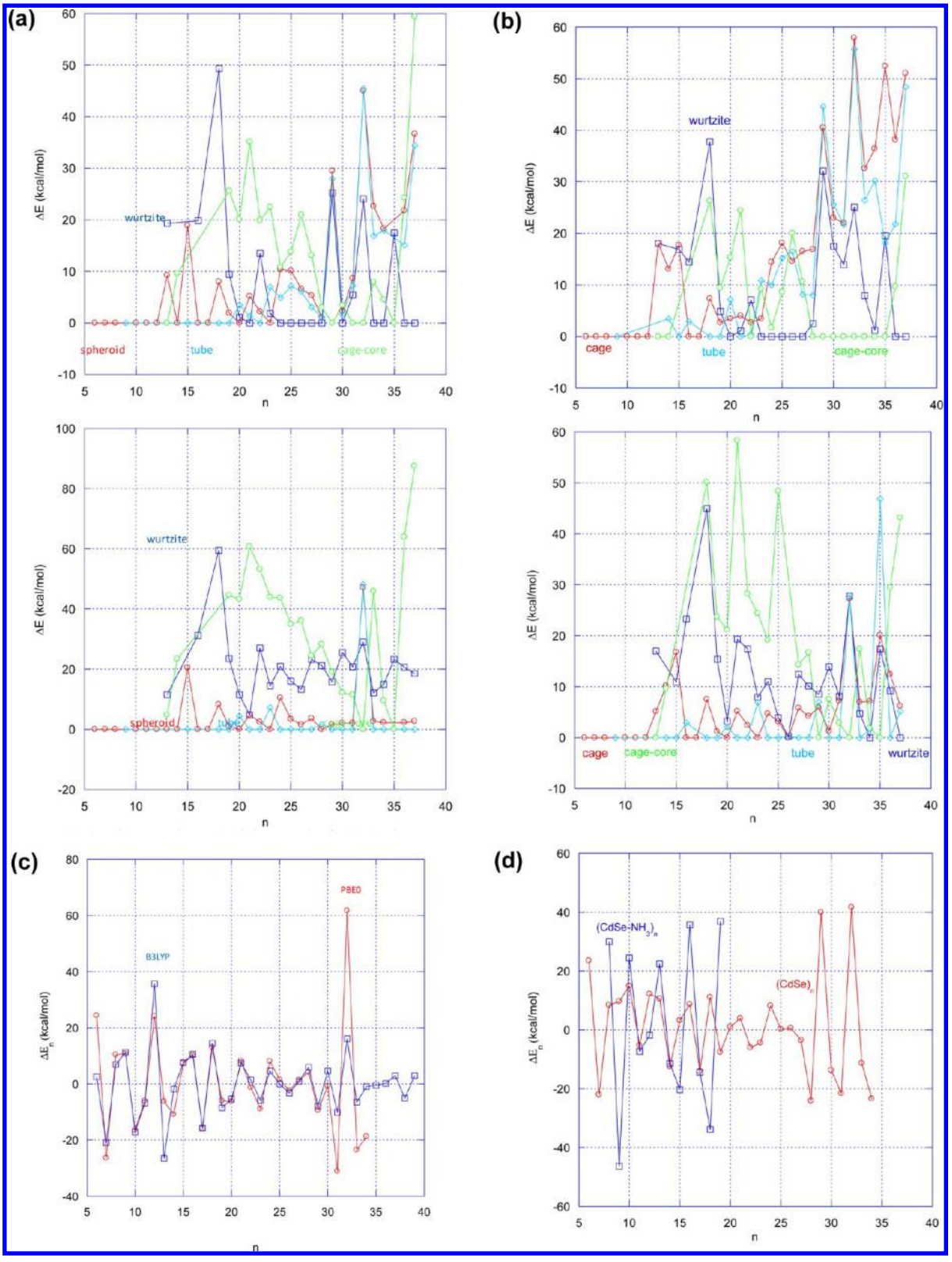

Figure 6. (a) PBE0 (top) and B3LYP (bottom) relative energies for $(ZnS)_n$ isomers. (b) PBE0 (top) and B3LYP (bottom) relative energies for $(CdSe)_n$ isomers. (c) Relative stability energies for for $(ZnS)_n$. (d) PBE0 relative stability energies.

given Table 7S (Supporting Information), which shows good agreement (MAE = 2.0 kcal/mol) between PBE0 and MP2 results. Except for n = 7, 13, and 14, clusters with n = 6−16 form cage structures in which all atoms are tricoordinated, as previously predicted.[10,22,32,45,69] Some of the $(CdSe)_n$ and $(ZnS)_n$ clusters have the same structural motifs (n = 6,8−13, 15−19, 23−27, 29−32, 35−37). Some of the B3LYP global minima predicted for $(ZnS)_n$ (n = 13, 21, 24−31, 33, 34, 36, 37) and $(CdSe)_n$ (n = 14, 20, 22−28, 30, 31, 33, 34, 36) clusters[32,45,69] are at variance with the PBE0 and MP2 results.

dx.doi.org/10.1021/ct4001944 | J. Chem. Theory Comput. 2013, 9, 3581−3596

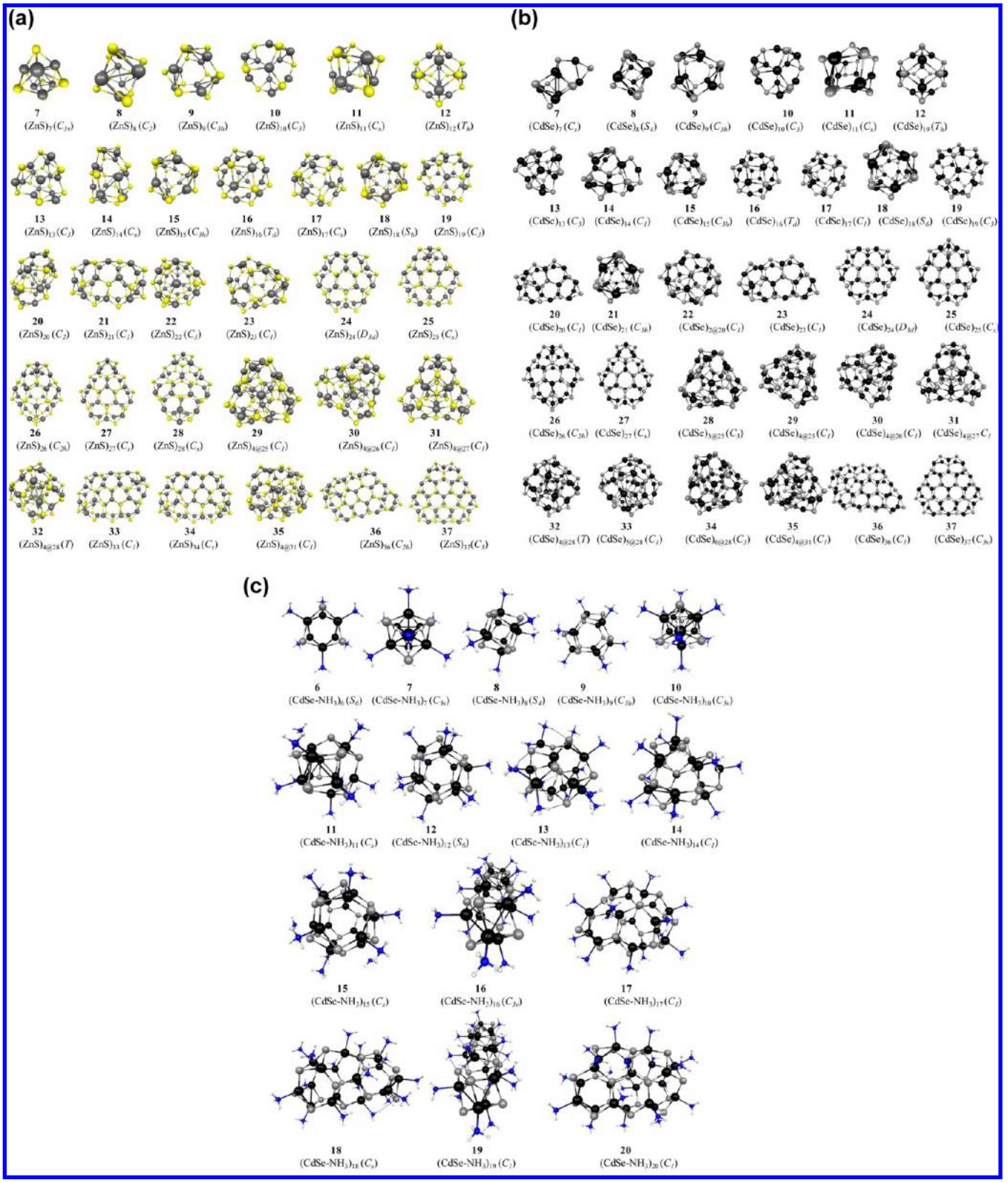

Figure 7. (a) PBE0 $(ZnS)_n$ structures. (b) PBE0 $(CdSe)_n$ structures. (c) PBE0 $(CdSe{-}NH_3)_n$ structures.

Our results confirm the C_3 cage−core global minimum reported for and $(CdSe)_{13}$[10,25,32,35] for both PBE0 and B3LYP functional (Figure 7b). This cage−core structure is also the PBE0 global minimum for $(ZnS)_{13}$ (Figure 7), but only a predicted[32,45,69] B3LYP local minimum. However, there are two local minima within 1−4 kcal/mol of the global minimum for n = 13. $(ZnS)_{14}$ adopted a cage structure[32,45,69] as predicted by PBE0 and B3LYP. For $(CdSe)_{14}$, the B3LYP cage structure with C_s symmetry,[22,32] is not the global minimum when using PBE0 functional. The PBE0 global minimum for $(CdSe)_{14}$ has a cage−core structure similar to the global minimum for $(CdSe)_{13}$. Note that clusters with n = 13, 14 have low relative

dx.doi.org/10.1021/ct4001944 | J. Chem. Theory Comput. 2013, 9, 3581−3596

stability energies (Figure 6d) compared to the T_h $(CdSe)_{12}$,[31,33] C_{3h} $(CdSe)_{15}$,[32] and T_d $(CdSe)_{16}$.[31,32] However, amine passivation leads to greater stability for $(CdSe)_{13}$ (vide infra). For n = 10 and 16, the ring structures obtained from a density functional tight binding method used for $(ZnS)_n$ clusters[70] are found to be very high in energy. For n = 16, there is a low-lying isomer with C_{3v} symmetry on the potential energy surface, about 3 kcal/mol higher than the LE T_d structure. The tubular structures for n = 15 originate from the smaller $(ZnS)_9$ and $(CdSe)_9$ clusters, similar to the (3, 3) armchair of carbon nanotube. For n < 17, the wurtzite-based structures considered previously for $(CdSe)_{13}$,[30,33] and $(CdSe)_{15}$,[38,71] $(CdSe)_{16}$,[33,34] and $(CdSe)_{17}$,[71,72] are significantly higher in energy compared to the corresponding cages.

The next larger $(ZnS)_{18}$[44,45,73] and $(CdSe)_{18}$ SNCs are predicted by PBE0 and B3LYP to be the (3, 3) armchair with the S_6 symmetry similar to those obtained for the corresponding (n = 18) group III−V clusters.[74] However, in contrast to the B3LYP results, the LE structures for the S_6 tubular motif predicted by PBE0 do not extend to larger (n + 6) clusters. With increasing cluster sizes, the wurtzite topology (n = 21, 23−28, 33, 34, 36, 37) and cage−core motifs (n = 29−32, 35) become more stable for $(ZnS)_n$ (cf. Figures 6 and 7). Similarly, global minima of CdSe SNCs for n = 20, 23−27, 36−37 were found to have a wurtzite morphology (Figures 6b and 7b). For $(CdSe)_n$ with n = 28−35, the cage−core motif becomes more stable than the wurtzite topology. For n = 28, $(CdSe)_{3@25}$ is the most stable while the wurtzite motif is the LE structure for $(ZnS)_{28}$. Structures with larger cubic cores are the lowest in energy for $(ZnS)_n$ with n = 29, 30, 32, 35 and for $(CdSe)_n$ with n = 29−32 35. For n = 33−34, the wurtzite is the most stable motif for ZnS clusters while the cage−core $(CdSe)_{5@28}$ and $(CdSe)_{6@28}$ are global minima as previously predicted.[10,35,75] The results are sensitive to the choice of functionals. B3LYP predicted these cage−cores to be much (17 and 27 kcal/mol) higher in energy than the corresponding lowest energy cages for $(CdSe)_{33}$ and $(CdSe)_{34}$, respectively. A structure for $(CdSe)_{33}$ constructed from a wurtzite lattice[27−29,38] is very high in energy (67.4 kcal/mol) relative to the lowest energy structure. For smaller cage−core structures with n = 32, the symmetric T cage and a cubic core provide the most stable structures for $(ZnS)_{4@28}$ and $(CdSe)_{4@28}$. The cubic core is also found to be stable inside the larger $(ZnS)_{31}$ and $(CdSe)_{31}$ cages for n = 35.

Passivated Clusters. There has been important progress recently in the synthesis and characterization of ligated $(CdSe)_n$ with various sizes, ranging from $(CdSe)_{13}$,[10,36] $(CdSe)_{19}$,[10,11,36] $(CdSe)_{33}$,[10−12,14,36] $(CdSe)_{34}$[10,14,36] and $(CdSe)_{48}$,[36] the smallest observed SNC reported as (CdSe-*n*-octylamine)$_{13}$.[11] Computational studies of the effects of passivating ligands have been carried for different $(CdSe)_n$ cluster sizes. Previous studies were mostly limited to clusters constructed from the wurtzite lattice[26−29,38] and small clusters.[24,25,30,76] Systematic amine passivation of $(CdSe)_n$ has not been reported. In the present study, the passivating effects of amines were primarily modeled with NH_3 per Cd site for global minima and low-lying local minima of bare $(CdSe)_n$, resulted in the full tetracoordination for the surface metals. For primary amines and other hydrogen bonded ligands, H−Se binding provides additional stability for some systems. Thus, the most stable passivated structures were found to have the saturation of dangling bonds of Cd atoms and H−Se bonds. The PBE0 errors obtained for the ground and excited states (Figures 1S and 2S of the Supporting Information) are comparable to values obtained for the hydrated clusters. Global minima for passivated $(CdSe-NH_3)_n$ with n = 8−9, 12−15, and 20 retain the motifs of their bare clusters (structures shown in Figure 7c). For some passivated clusters, different competing topologies arise due to the present of H−Se interactions, as found in the tubular topology for n = 10, 16, and 19. The passivated minima of LE bare clusters are 6.0, 24.4, and 35.5 kcal/mol higher in energy than the global minima for n = 10, 16, and 19, respectively. For n = 13, the long C_{3v} tubular structure, locating at 47 kcal/mol higher than the $(CdSe)_{13}$ global minimum, are about 7 kcal/mol higher in energy after (NH_3) passivation. Passivating with (NH_2CH_3) reduces the gap to about 4 kcal/mol. Solvation also induces a modest shift, resulting in a difference of about 1 kcal/mol between to two lowest energies $(CdSe-NH_2CH_3)_{13}$ isomers. Thus, key factors in thermostability for $(CdSe)_n$ include the effects solvation and specific ligand interactions that might allow topology control. Note that the magnitudes of the calculated thermostability for $(CdSe-NH_3)_n$ are significantly larger than the corresponding bare clusters.

B.2. One-Photon Absorption Spectra. The excited states formed a basic picture of how size and shape control OPA spectra of bare and amine passivated CdSe clusters, as has been discussed for the tubular and wurtzite topologies.[22] However, note that the predicted results have been qualitatively assessed in comparison to optical absorption data from mixtures of SNCs due to the lack of experimental data from discrete and pure nanoclusters. Access to recent OPA data[11,12] of purified $[(CdSe)$-(*n*-octylamine)$]_{13}$ allows a detailed comparison with TDDFT results, as shown in Figure 8. The experimental

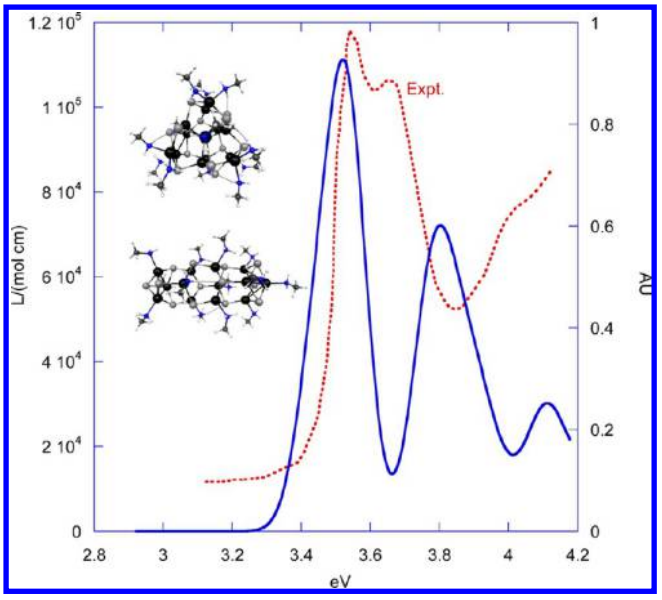

Figure 8. Computed Boltzmann averaged OPA spectrum for two $(CdSe-NH_2CH_3)_{13}$ isomers compared with the experimental spectrum (ref 11) of $[(CdSe)-n$-octylamine$]_{13}$.

spectrum of $[(CdSe)$-(*n*-octylamine)$]_{13}$ in toluene exhibits two maxima, at 3.54 (350) and 3.70 eV (335 nm), and a shoulder at 3.97 eV, in agreement with an experimental spectrum previously assigned[11] to $(CdSe)_{13}$ clusters. Interestingly, the spectral assignment of $[(CdSe)$-(*n*-octylamine)$]_{13}$ was fortuitously based in part on TD-PW91 calculations for a $(CdSe)_{13}$ cluster with 6 formate-hydrogen pairs,[29] although elemental

dx.doi.org/10.1021/ct4001944 | J. Chem. Theory Comput. 2013, 9, 3581−3596

analyses by laser-desorption-ionization (LDI) mass spectrometry established the empirical formula and the IR spectrum showed "no residual acetate or water absorptions".[11] This calls for further investigation of the validity of $(CdSe)_{13}$ with formate−hydrogen pairs model.[29] PBE0 calculations (see Table 7S in the Supporting Information) predict the first excitation energy of $(CdSe)_{13}$ cluster with six formate−hydrogen pairs of about 3.9 eV, much higher than the first observed peak at 3.54 eV of $[(CdSe)-(n\text{-octylamine})]_{13}$. The predicted absorption spectrum for $(CdSe\text{-methylamine})_{13}$ has three peaks at 3.53, 3.80, and 4.11 eV. The first predicted absorption peak closely matches experiment while the slightly overestimated second peak creates a spectral profile with a deeper minimum between the first two maxima. The first band is made up of three lowest transitions, originating mainly from the highest occupied MO (HOMO), HOMO − 1, and HOMO − 2 to the lowest unoccupied MO (LUMO) excitations, respectively. The occupied MOs comprise mainly of by π-orbitals from Se atoms while the virtual orbital does have significantly contributions from the nitrogen lone pairs (see Supporting Information Figures 6S and 7S). The effects of amines appear to be well-approximated by NH_3 with similar excited transition levels (see Table 8S of the Supporting Information), in agreement with previous studies.[22,24] The first excitation energy of about 3.0 eV was previously predicted for $(CdSe)_{13}-(NH_3)_{10}$ at the TD-B3LYP/LANL2DZ level.[25]

Although isolation and optical characterization of larger purified SNCs have not been reported, higher-mass peaks in the LDI spectrum $[(CdSe)-(n\text{-octylamine})]_{13}$ were assigned to $(CdSe)_{19}$, $(CdSe)_{33}$, and $(CdSe)_{34}$, due to thermal heating and subsequent growth of $(CdSe)_{13}$.[11] The first absorption peaks, however, have been assigned for $(CdSe)_{19}$ (4.42 eV, 363 nm), $(CdSe)_{33,34}$ (3.19 eV, 389 nm), and $(CdSe)_{66}$ (3.00 eV, 413 nm) in the spectral evolution of CdSe nanoclusters.[12] Absorption spectra were also reported for mass-selected mixture of $(CdSe)_{33,34}$ (2.99 eV, 415 nm)[10] and $(CdSe)_{34}$ (3.02 eV, 410 nm)[77] NPs grown in solution with amine ligands. Interestingly, L-cysteine capped $(CdSe)_{33,34}$ (2.95 eV, 420 nm)[14] grown in aqueous solution and CdSe NPs capped with other ligands[4,78] were also reported to have similar absorption features to the corresponding colloidal mixture amine-capped NPs. To compare with experimental spectra assigned to amine ligated nanoclusters in solutions, TDDFT calculations with the PCM solvation model were carried out for low-energy isomers of NH_3 passivated $(CdSe)_{19}$, $(CdSe)_{33}$, and $(CdSe)_{34}$.

For $(CdSe)_{19}$, the first excited states are predicted to be about 3.2 eV ($f = 0.21$) and 3.3 eV ($f = 0.42$) for the passivated structures capped with 19 and 18 NH_3 molecules, respectively. The predicted values are in reasonable agreement with first absorption peak of 4.42 eV assigned to $(CdSe)_{19}-n$-octylamine.[12] Although the $(CdSe)_{19}-18NH_3$ constructed from a wurtzite lattice can be ruled out due to the high (30 kcal/mol relative to the lowest wurtzite structure of $(CdSe)_{19}-18NH_3$) ground state energy, excited calculations were carried out for comparison. The weakly absorbing ($f = 0.07$) lowest excited state of about 3.0 eV was obtained for the previously proposed $(CdSe)_{19}-18NH_3$. Thus, $(CdSe)_{13}$ and $(CdSe)_{19}$ structures constructed using a wurtzite lattice[29] without using global optimization methods appear to be unfit for a priori predictions. It also appears to be true for the proposed[28,29,38] structure for the larger $(CdSe)_{33}$ cluster (vide supra).

Previous estimates for the first excited state of about 3 eV for the wurtzite structure of $(CdSe)_{33}$ with 21 NH_2CH_3 ligands were carried out using ground state orbital energies,[28] and later,[27] TDDFT. Del Ben et al.[29] reported good agreement (after a 0.43 eV correction) with experiment using PW91 functional for the same structural motif but with 21 NH_3 ligands. In order to avoid fortuitous agreement with experiment, we consider different motifs and account for spectral intensities and higher transitions as the lowest transition energies for some of these systems agree reasonably well with experimental spectra. The experimental and our computed spectra for ligated $(CdSe)_{33}$ and $(CdSe)_{34}$ are shown in Figure 9. The sharp and intense spectral profile of the wurtzite structure of $(CdSe)_{33}-25NH_3$ shows good agreement with SNCs grown at 318 K. The first predicted absorption peak at 3.26 eV is in good agreement with experimental values of 2.99−3.19 eV.[10,12,77] Other cage−core motifs and wurtzite structures, including the $(CdSe)_{33}-21NH_3$ structure constructed using a wurtzite lattice,[29] were also considered. Spectra computed for other ligated $(CdSe)_{33}$ and $(CdSe)_{34}$ topologies (Figure 8S−11S of the Supporting Information) do not match the reported spectra.[10,77] In comparison with the spectra for the wurtzite structure of $(CdSe)_{33}-25NH_3$ (Figure 9a), previously proposed[10] cage−core structures of $(CdSe)_{5@28}-28NH_3$ (Figure 9b), $(CdSe)_{6@28}-28NH_3$ (Figure 9c), $(CdSe)_{3@30}-28NH_3$ (Figure 8S of the Supporting Information), and $(CdSe)_{33}-21NH_3$ constructed from wurtzite lattice (Figure 9S in the Supporting Information) have markedly different profiles. The cage−core systems (Figure 9b and c) have lower energy absorption peaks for the first bands. These spectral profiles have features that are somewhat similar to the spectrum for the larger SNCs prepared at higher temperature with a broad first absorption peak at 2.58 eV (480 nm).[10] Finally, interestingly, prediction of the exciton binding energy, given as the difference between the fundamental gap (IP-EA, see Table 5) and the excitation energy, results in values of about 1 eV, consistent with X-ray absorption and photoemission spectra for CdSe QDs.[79]

4. SUMMARY AND CONCLUSIONS

One of the main challenges in predicting optical properties of semiconductor nanoclusters involves identifying effective methods for structure determination, which involves locating global minima among the larger number of possible isomers with increasing cluster size. With a suitable functional, DFT can provide an effective tool at relatively low computational cost for predicting structures of nanoclusters for excited state calculations with TDDFT. Thus, a systematic coupled-cluster study for the ground and excited states of bare and hydrated ZnS and CdSe clusters was carried out to evaluate the performance of functionals for DFT and TDDFT.

The results suggest that the popular B3LYP functional does not deliver optimal results for the ground and excited state. The PBE0 functional was found to provide a better description for both the ground and excited states for small bare $(ZnS)_n$ and bare and ligated $(CdSe)_n$ clusters. The results were found to deteriorate for the hydrated ZnS clusters, due the presence of CT transitions. However, the errors decrease with increasing cluster size. Although large errors for $(ZnS-2H_2O)_2$ and $(ZnS-2H_2O)_3$ were obtained with PBE0, the errors for larger hydrated ZnS clusters are not out of the typical (0.25 eV) range. PBE0 excitation energies are generally higher than the B3LYP values due to the HF exchange and GGA part of the functional. Increasing the amount of HF exchange, which is important for proper treatment of systems with CT character,

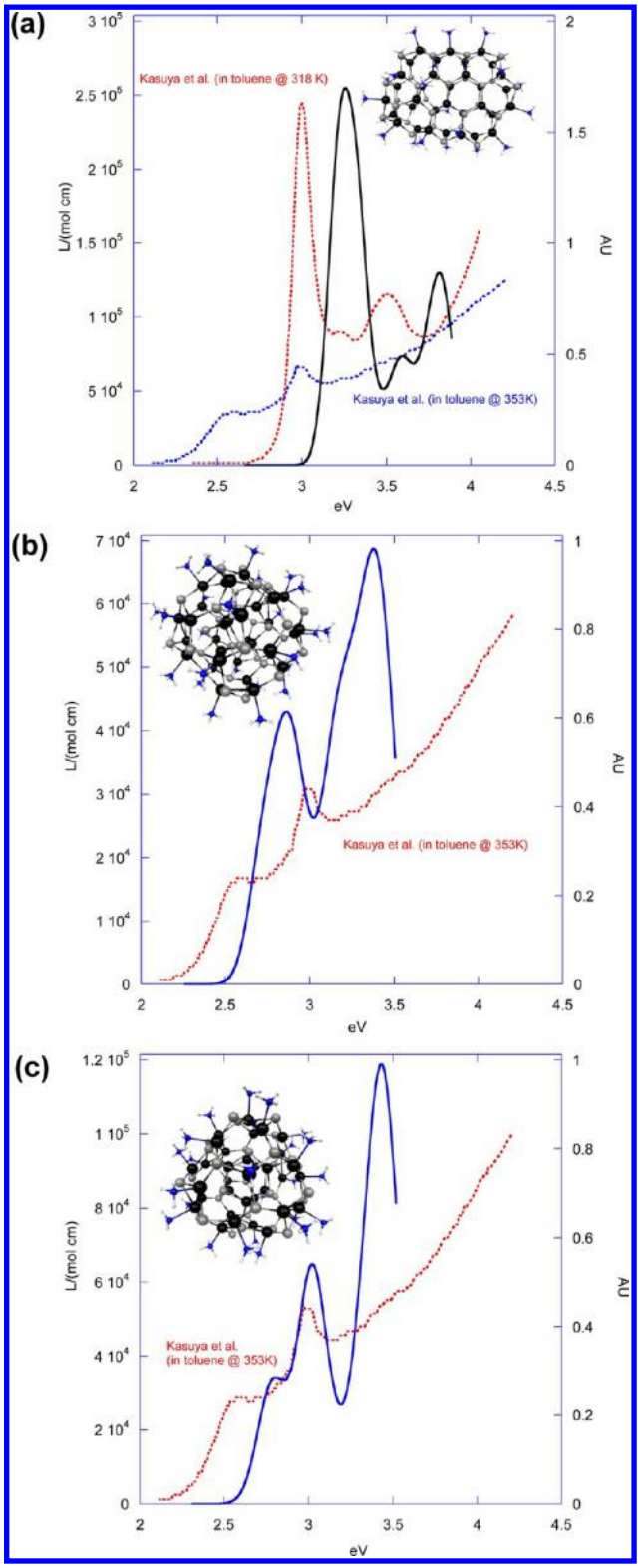

Figure 9. Computed OPA spectrum for (a) $[(CdSe)_{33}-25NH_3$ compared with experimental (ref 10) spectra; (b) $[(CdSe)_{5@28}-28NH_3$ compared with experimental (ref 10) spectrum; (c) $[(CdSe)_{6@28}-28NH_3$ compared with experimental (ref 10.) spectrum.

generally increases the predicted excitation energies. The excitation energies from the PBE exchange-correlation functional are typically higher than the corresponding BLYP values. Excitation energies obtained with the long-range hybrid CAM-B3LYP and CA-B3LYP were found to provide more consistent results for both small anhydrous and hydrated ZnS clusters. However, their performance in spectral predictions for larger clusters requires further study due to the presence of varying degrees of CT character in different systems, which require different amounts HF exchange. Thus, functionals such as CA-B3LYP that provide good estimates for modest CT transitions have significant errors for strong CT excitations. Functionals that provide accurate long-range CT excitation energies overestimate local or weak CT transitions. Thus, we stress that no functional, including the CAM-B3LYP and CA-B3LYP, are likely to be the best for all ligated ZnS clusters.

Table 5. PBE0 Vertical Ionization Potential (IP = $E^+ - E$) and Electron Affinity (EA = $E - E^-$), as well as Exciton Binding Energy (EBE = IP − EA − S_1) Energies (eV)[a]

	gas-phase			toluene		
system	IP	EA	EBE	IP	EA	EBE
$(CdSe)_{13}-13NH_3$	5.25	−0.20	2.28	4.90	0.55	1.05
$(CdSe)_{33}-25NH_3$	5.11	0.26	1.74	4.83	0.84	0.83

[a] E, E^+, and E^- are total energies of the neutral, cation, and anion species, respectively.

In an effort to study the influence of topology, size, and ligands on optical properties of realistic ultrasmall nanoclusters, structures and electronic excitation calculations have been carried out for bare and amine ligated $(CdSe)_n$ clusters. Except for the cage−core structures of $(ZnS)_{13}$, $(CdSe)_{13}$, and $(CdSe)_{14}$, small bare ZnS and CdSe clusters are predicted to be spheroids and tubular structures (8−12, 15−19) with squares and hexagons, similar to the structures of carbon single-wall nanotubes. Wurtzite (n = 23−27, 36, 37) and cage−core (n = 28−35) structures are generally more stable for larger clusters. Bare $(ZnS)_n$ and $(CdSe)_n$ with n = 32 were found to have the highest relative stability. These clusters were predicted to have cubic cores (4@28). With one amine per metal, small ligated (n = 8−9, 12−15, 20) clusters were found to retain the motifs of their bare counterparts. Due to H−Se bonding, different competing topologies arise in some passivated clusters. Spectral profiles predicted by TDDFT with the PCM solvation model using PBE0 functional for $(CdSe\text{-methylamine})_{13}$ and the larger ligated $(CdSe)_{33}$ are consistent with the experimental spectra. Thus, the same methodology might be applicable for larger bare and ligated CdSe and bare ZnS nanoparticles.

■ ASSOCIATED CONTENT

Supporting Information

Computed excitation energies, spectra, molecular orbitals, structures, and relative energies for $(ZnS)_n$ and $(CdSe)_n$. This material is available free of charge via the Internet at http://pubs.acs.org.

■ AUTHOR INFORMATION

Corresponding Author

*E-mail: Kiet.Nguyen@wpafb.af.mil (K.A.N.), Ruth.Pachter@wpafb.af.mil (R.P.).

Notes

The authors declare no competing financial interest.

■ ACKNOWLEDGMENTS

This research has been supported by the Air Force Office of Scientific Research and by CPU time from the Air Force Research Laboratory DoD Supercomputing Resource Center.

■ REFERENCES

(1) Brus, L. E. *J. Chem. Phys.* **1984**, *80*, 4403.
(2) Brus, L. *J. Phys. Chem.* **1986**, *90*, 2555.
(3) Alivisatos, A. P.; Harris, A. L.; Levinos, N. J.; Steigerwald, M. L.; Brus, L. E. *J. Chem. Phys.* **1988**, *89*, 4001.
(4) Murray, C. B.; Norris, D. J.; Bawendi, M. G. *J. Am. Chem. Soc.* **1993**, *115*, 8706.
(5) Scholes, G. D. *Adv. Funct. Mater.* **2008**, *18*, 1157.
(6) He, G. S.; Yong, K.-T.; Zheng, Q.; Sahoo, Y.; Baev, A.; Ryasnyanskiy, A. I.; Prasad, P. N. *Opt. Express* **2007**, *15*, 12818.
(7) Padilha, L. A.; Fu, J.; Hagan, D. J.; W., V. S. E.; Cesar, C. L.; Barbosa, L. C.; Cruz, C. H. B.; Buso, D.; Martucci, A. *Phys. Rev. B: Condens. Matter Mater. Phys.* **2007**, *75*, 075325/1.
(8) Cossairt, B. M.; Owen, J. S. *Chem. Mater.* **2011**, *23*, 3114.
(9) Newton, J. C.; Ramasamy, K.; Mandal, M.; Joshi, G. K.; Kumbhar, A.; Sardar, R. *J. Phys. Chem. C* **2012**, *116*, 4380.
(10) Kasuya, A.; Sivamohan, R.; Barnakov, Y. A.; Dmitruk, I. M.; Nirasawa, T.; Romanyuk, V.; Kumar, V.; Mamykin, S. V.; Tohji, K.; Jeyadevan, B.; Shinoda, K.; Kudo, T.; Terasaki, O.; Liu, Z.; Belosludov, R. V.; Sundararajan, V.; Kawazoe, Y. *Nat. Mater.* **2004**, *3*, 99.
(11) Wang, Y.; Liu, Y.-H.; Zhang, Y.; Wang, F.; Kowalski, P. J.; Rohrs, H. W.; Loomis, R. A.; Gross, M. L.; Buhro, W. E. *Angew. Chem., Int. Ed.* **2012**, *51*, 6154.
(12) Liu, Y.-H.; Wang, F.; Wang, Y.; Gibbons, P. C.; Buhro, W. E. *J. Am. Chem. Soc.* **2011**, *133*, 17005.
(13) Chestnoy, N.; Hull, R.; Brus, L. E. *J. Chem. Phys.* **1986**, *85*, 2237.
(14) Park, Y.-S.; Dmytruk, A.; Dmitruk, I.; Kasuya, A.; Okamoto, Y.; Kaji, N.; Tokeshi, M.; Baba, Y. *J. Phys. Chem. C* **2010**, *114*, 18834.
(15) Rossetti, R.; Hull, R.; Brus, L. E. *J. Chem. Phys.* **1985**, *82*, 522.
(16) Nakaoka, Y.; Nosaka, Y. *Langmuir* **1997**, *13*, 708.
(17) Yu, K. *Adv. Mater. (Weinheim, Ger.)* **2012**, *24*, 1123.
(18) Evans, C. M.; Love, A. M.; Weiss, E. A. *J. Am. Chem. Soc.* **2012**, *134*, 17298.
(19) (a) Liu, C.; Chung, S.-Y.; Lee, S.; Weiss, S.; Neuhauser, D. *J. Chem. Phys.* **2009**, *131*, 174705. (b) Troparevsky, M. C.; Kronik, L.; Chelikowsky, J. R. *Phys. Rev. B* **2001**, *65*, 033311/1.
(20) Chung, S.-Y.; Lee, S.; Liu, C.; Neuhauser, D. *J. Phys. Chem. B* **2009**, *113*, 292.
(21) Kim, H.-S.; Jang, S.-W.; Chung, S.-Y.; Lee, S.; Lee, Y.; Kim, B.; Liu, C.; Neuhauser, D. *J. Phys. Chem. B* **2010**, *114*, 471.
(22) Nguyen, K. A.; Day, P. N.; Pachter, R. *J. Phys. Chem. C* **2010**, *114*, 16197.
(23) Lim, E.; Kuznetsov, A. E.; Beratan, D. N. *Chem. Phys.* **2012**, *407*, 97.
(24) Kuznetsov, A. E.; Balamurugan, D.; Skourtis, S. S.; Beratan, D. N. *J. Phys. Chem. C* **2012**, *116*, 6817.
(25) Yang, P.; Tretiak, S.; Ivanov, S. *J. Cluster Sci.* **2011**, *22*, 405.
(26) Fischer, S. A.; Crotty, A. M.; Kilina, S. V.; Ivanov, S. A.; Tretiak, S. *Nanoscale* **2012**, *4*, 904.
(27) Albert, V. V.; Ivanov, S. A.; Tretiak, S.; Kilina, S. V. *J. Phys. Chem. C* **2011**, *115*, 15793.
(28) Kilina, S.; Ivanov, S.; Tretiak, S. *J. Am. Chem. Soc.* **2009**, *131*, 7717.
(29) Del Ben, M.; Havenith, R. W. A.; Broer, R.; Stener, M. *J. Phys. Chem. C* **2011**, *115*, 16782.
(30) Jose, R.; Zhanpeisov, N. U.; Fukumura, H.; Baba, Y.; Ishikawa, M. *J. Am. Chem. Soc.* **2006**, *128*, 629.
(31) Matxain, J. M.; Mercero, J.; Fowler, J. E.; Ugalde, J. M. *J. Phys. Chem. A* **2004**, *108*, 10502.
(32) Sanville, E.; Burnin, A.; BelBruno, J. J. *J. Phys. Chem. A.* **2006**, *110*, 2378.
(33) Jha, P. C.; Seal, P.; Sen, S.; Agren, H.; Chakrabarti, S. *Comput. Mater. Sci.* **2008**, *44*, 728.
(34) Deglmann, P.; Ahlrichs, R.; Tsereteli, K. *J. Chem. Phys.* **2002**, *116*, 1585.
(35) Botti, S.; Marques, M. A. L. *Phys. Rev. B* **2007**, *75*, 035311.
(36) Romanyuk, V. R.; Dmitruk, I. M.; Barnakov, Y. A.; Belosludov, R. V.; Kasuya, A. *J. Nanosci. Nanotechnol.* **2009**, *9*, 2111.
(37) Voznyy, O. *J. Phys. Chem. C* **2011**, *115*, 15927.
(38) Puzder, A.; Williamson, A. J.; Gygi, F.; Galli, G. *Phys. Rev. Lett.* **2004**, *92*, 217401.
(39) Azpiroz, J. M.; Lopez, X.; Ugalde, J. M.; Infante, I. *J. Phys. Chem. C* **2012**, *116*, 2740.
(40) Malloci, G.; Chiodo, L.; Rubio, A.; Mattoni, A. *J. Phys. Chem. C* **2012**, *116*, 8741.
(41) Azpiroz, J. M.; Infante, I.; Lopez, X.; Ugalde, J. M.; De, A. F. *J. Mater. Chem.* **2012**, *22*, 21453.
(42) Zwijnenburg, M. A.; Illas, F.; Bromley, S. T. *Phys. Chem. Chem. Phys.* **2011**, *13*, 9311.
(43) Zwijnenburg, M. A.; Sousa, C.; Illas, F.; Bromley, S. T. *J. Chem. Phys.* **2011**, *134*, 064511/1.
(44) Zwijnenburg, M. A. *Nanoscale* **2011**, *3*, 3780.
(45) Hamad, S.; Catlow, C. R. A.; Spano, E.; Matxain, J. M.; Ugaldeora, J. M. *J. Phys. Chem. B* **2005**, *109*, 2703.
(46) Spano, E.; Hamad, S.; Catlow, C. R. A. *J. Phys. Chem. B* **2003**, *107*, 10337.
(47) Matxain, J. M.; Irigoras, A.; Fowler, E. J.; Ugalde, J. M. *Phys. Rev. A* **2000**, *63*, 013202.
(48) Matxain, J. M.; Irigoras, A.; Fowler, J. E.; Ugalde, J. M. *Phys. Rev. A* **2001**, *64*, 013201.
(49) Hirata, S.; Fan, P.-D.; Auer, A.; Nooijen, M.; Piecuch, P. *J. Chem. Phys.* **2004**, *121*, 12197.
(50) Christiansen, O.; Koch, H.; Jorgensen, P. *Chem. Phys. Lett.* **1995**, *243*, 409.
(51) Balabanov, N. B.; Peterson, K. A. *J. Chem. Phys.* **2005**, *123*, 064107.
(52) Martin, J. M. L.; Sundermann, A. *J. Chem. Phys.* **2001**, *114*, 3408.
(53) Vailev, M.; Bylaska, E. J.; Govind, N.; Kowalski, K.; Straatsma, T. P.; van Dam, H. J. J.; Wang, D.; Nieplocha, J.; Apra, E.; Windus, T. L.; de Jong, W. A. *Comput. Phys. Commun.* **2010**, *181*, 1477.
(54) Kohn, W.; Sham, L. J. *Phys. Rev.* **1965**, *140*, A1133.
(55) Frisch, M. J.; Trucks, G. W.; Schlegel, H. B.; Scuseria, G. E.; Robb, M. A.; Cheeseman, J. R.; Montgomery, J. A., Jr.; Vreven, T.; Kudin, K. N.; Burant, J. C.; Millam, J. M.; Iyengar, S. S.; Tomasi, J.; Barone, V.; Mennucci, B.; Cossi, M.; Scalmani, G.; Rega, N.; Petersson, G. A.; Nakatsuji, H.; Hada, M.; Ehara, M.; Toyota, K.; Fukuda, R.; Hasegawa, J.; Ishida, M.; Nakajima, T.; Honda, Y.; Kitao, O.; Nakai, H.; Klene, M.; Li, X.; Knox, J. E.; Hratchian, H. P.; Cross, J. B.; Adamo, C.; Jaramillo, J.; Gomperts, R.; Stratmann, R. E.; Yazyev, O.; Austin, A. J.; Cammi, R.; Pomelli, C.; Ochterski, J. W.; Ayala, P. Y.; Morokuma, K.; Voth, G. A.; Salvador, P.; Dannenberg, J. J.; Zakrzewski, V. G.; Dapprich, S.; Daniels, A. D.; Strain, M. C.; Farkas, O.; Malick, D. K.; Rabuck, A. D.; Raghavachari, K.; Foresman, J. B.; Ortiz, J. V.; Cui, Q.; Baboul, A. G.; Clifford, S.; Cioslowski, J.; Stefanov, B. B.; Liu, G.; Liashenko, A.; Piskorz, P.; Komaromi, I.; Martin, R. L.; Fox, D. J.; Keith, T.; Al-Laham, M. A.; Peng, C. Y.; Nanayakkara, A.; Challacombe, M.; Gill, P. M. W.; Johnson, B.; Chen, W.; Wong, M. W.; Gonzalez, C.; Pople, J. A. *Gaussian*, A.11.4 ed.; Gaussian, Inc.: Pittsburgh, PA, 2003.
(56) Schmidt, M. W.; Baldridge, K. K.; Boatz, J. A.; Elbert, S. T.; Gordon, M. S.; Jensen, J. H.; Koseki, S.; Matsunaga, N.; Nguyen, K. A.; Su, S.; Windus, T. L.; Dupuis, M.; Montgomery, J. A. *J. Comput. Chem.* **1993**, *14*, 1347.
(57) Nguyen, K. A.; Day, P. N.; Pachter, R. *J. Chem. Phys.* **2011**, *135*, 074109/1.
(58) Cossi, M.; Scalmani, G.; Rega, N.; Barone, V. *J. Chem. Phys.* **2002**, *117*, 43.
(59) Cossi, M.; Barone, V. *J. Chem. Phys.* **2001**, *115*, 4708.
(60) Nguyen, K. A.; Day, P. N.; Pachter, R. *J. Phys. Chem. A* **2009**, *113*, 13943.
(61) Andrae, D.; Haeussermann, U.; Dolg, M.; Stoll, H.; Preuss, H. *Theor. Chim. Acta* **1990**, *77*, 123.

(62) Bergner, A.; Dolg, M.; Kuchle, W.; Stoll, H.; Preuss, H. *Mol. Phys.* **1993**, *80*, 1431.
(63) Dolg, M.; Wedig, U.; Stoll, H.; Preuss, H. *J. Chem. Phys.* **1987**, *86*, 866.
(64) Hehre, W. J.; Ditchfield, R.; Pople, J. A. *J. Chem. Phys.* **1972**, *56*, 2257.
(65) Francl, M. M.; Petro, W. J.; Hehre, W. J.; Binkley, J. S.; Gordon, M. S.; DeFrees, D. J.; Pople, J. A. *J. Chem. Phys.* **1982**, *77*, 3654.
(66) Kumbhojkar, N.; Nikesh, V. V.; Kshirsagar, A.; Mahamuni, S. *J. Appl. Phys.* **2000**, *88*, 6260.
(67) Nikesh, V. V.; Dharmadhikari, A.; Ono, H.; Nozaki, S.; Kumar, G. R.; Mahamuni, S. *Appl. Phys. Lett.* **2004**, *84*, 4602.
(68) Mahamuni, S.; Khosravi, A. A.; Kundu, M.; Kshirsagar, A.; Bedekar, A.; Avasare, D. B.; Singh, P.; Kulkarni, S. K. *J. Appl. Phys.* **1993**, *73*, 5237.
(69) Burnin, A.; Sanville, E.; BelBruno, J. J. *J. Phys. Chem. A* **2005**, *109*, 5026.
(70) Pal, S.; Sharma, R.; Goswami, B.; Sarkar, P.; Bhattachryya, S. P. *J. Chem. Phys.* **2009**, *130*, 214703.
(71) Inerbaev, T. M.; Masunov, A. E.; Khodaker, S. I.; Dobrinescu, A.; Plamada, A.-V.; Kawazoe, Y. *J. Chem. Phys.* **2009**, *131*, 044106.
(72) Troparevsky, M. C.; Kronik, L.; Chelikowsky, J. R. *J. Chem. Phys.* **2003**, *119*, 2284.
(73) Matxain, J. M.; Eriksson, L. A.; Mercero, J. M.; Ugalde, J. M.; Spano, E.; Hamad, S.; Catlow, C. R. A. *Nanotechnology* **2006**, *17*, 4100.
(74) Shevlin, S. A.; Guo, Z. X.; van Dam, H. J. J.; Sherwood, P.; Catlow, C. R. A.; Sokol, A. A.; Woodley, S. M. *Phys. Chem. Chem. Phys.* **2008**, *10*, 1944.
(75) Wang, B.; Wang, X.; Zhao, J. *J. Phys. Chem. C* **2010**, *114*, 5741.
(76) Yang, P.; Tretiak, S.; Masunov, A. E.; Ivanov, S. *J. Chem. Phys.* **2008**, *129*, 074709/1.
(77) Yu, J. H.; Liu, X.; Kweon, K. E.; Joo, J.; Park, J.; Ko, K.-T.; Lee, D. W.; Shen, S.; Tivakornsasithorn, K.; Son, J. S.; Park, J.-H.; Kim, Y.-W.; Hwang, G. S.; Dobrowolska, M.; Furdyna, J. K.; Hyeon, T. *Nat. Mater.* **2009**, *9*, 47.
(78) Ptatschek, V.; T., S.; Lerch, M.; Muller, G.; Spanhel, L.; Emmerling, A.; Fricke, J.; Foitzik, A. H.; Langer, E. *Ber. Bunsenges. Phys. Chem.* **1998**, *102*, 85.
(79) Meulenberg, R. W.; Lee, J. R. I.; Wolcott, A.; Zhang, J. Z.; Terminello, L. J.; van, B. T. *ACS Nano* **2009**, *3*, 325.